

# On the sources and sinks of atmospheric VOCs: An integrated analysis of recent aircraft campaigns over North America

Xin Chen<sup>1</sup>, Dylan B. Millet<sup>1</sup>, Hanwant B. Singh<sup>2</sup>, Armin Wisthaler<sup>3,4</sup>, Eric C. Apel<sup>5</sup>, Elliot L. Atlas<sup>6</sup>, Donald R. Blake<sup>7</sup>, Ilann Bourgeois<sup>8,9</sup>, Steven S. Brown<sup>8</sup>, John D. Crouse<sup>10</sup>, Joost A. de Gouw<sup>8,9</sup>, Frank Flocke<sup>5</sup>, Alan Fried<sup>11</sup>, Brian G. Heikes<sup>12</sup>, Rebecca S. Hornbrook<sup>5</sup>, Tomas Mikoviny<sup>4</sup>, Kyung-Eun Min<sup>13</sup>, Markus Müller<sup>3,\*</sup>, J. Andrew Neuman<sup>8,9</sup>, Daniel W. O'Sullivan<sup>14</sup>, Jeff Peischl<sup>8,9</sup>, Gabriele G. Pfister<sup>5</sup>, Dirk Richter<sup>11</sup>, James M. Roberts<sup>8</sup>, Thomas B. Ryerson<sup>8</sup>, Stephen Shertz<sup>15</sup>, Chelsea R. Thompson<sup>8,9</sup>, Victoria Treadaway<sup>12</sup>, Patrick R. Veres<sup>8</sup>, James Walega<sup>11</sup>, Carsten Warneke<sup>8,9</sup>, Rebecca A. Washenfelder<sup>8</sup>, Petter Weibring<sup>11</sup>, Bin Yuan<sup>16</sup>

<sup>1</sup>Department of Soil, Water, and Climate, University of Minnesota, Minneapolis-Saint Paul, MN 55108, USA

<sup>2</sup>NASA Ames Research Center, Moffett Field, CA, USA

<sup>3</sup>Institute for Ion Physics and Applied Physics, University of Innsbruck, 6020 Innsbruck, Austria

<sup>4</sup>Department of Chemistry, University of Oslo, Norway

<sup>5</sup>Atmospheric Chemistry Observations & Modeling Laboratory, National Center for Atmospheric Research, Boulder, CO, 80301, USA

<sup>6</sup>Department of Atmospheric Sciences, Rosenstiel School of Marine and Atmospheric Science, University of Miami, Miami, FL, USA

<sup>7</sup>Department of Chemistry, University of California, Irvine, Irvine, CA, USA

<sup>8</sup>Chemical Sciences Division, NOAA Earth System Research Laboratory, Boulder, CO 80305, USA

<sup>9</sup>Cooperative Institute for Research in Environmental Sciences, University of Colorado, Boulder, CO 80309, USA

<sup>10</sup>Division of Geological and Planetary Sciences, California Institute of Technology, Pasadena, CA 91125, USA

<sup>11</sup>Institute of Arctic & Alpine Research, University of Colorado, Boulder, CO

<sup>12</sup>Graduate School of Oceanography, University of Rhode Island, Narragansett, RI 02882, USA

<sup>13</sup>School of Earth Science and Environmental Engineering, Gwangju Institute of Science and Technology

<sup>14</sup>United States Naval Academy, Chemistry Department, Annapolis, MD, 21401, USA

<sup>15</sup>Atmospheric Chemistry Division, National Center for Atmospheric Research, Boulder, Colorado, USA

<sup>16</sup>Institute for Environmental and Climate Research, Jinan University, Guangzhou, China

\*now at: Ionicon Analytik GmbH, Innsbruck, Austria

Correspondence to: Dylan B. Millet (dbm@umn.edu)

## Abstract

We apply a high-resolution chemical transport model (GEOS-Chem CTM) with updated treatment of volatile organic compounds (VOCs) and a comprehensive suite of airborne datasets over North America to i) characterize the VOC budget, and ii) test the ability of current models to capture the distribution and reactivity of atmospheric VOCs, over this region. Biogenic emissions dominate the North American VOC budget in the model, accounting for 70% and 95% of annually emitted VOC-carbon and reactivity, respectively. Based on current inventories anthropogenic emissions have declined to the point where biogenic emissions are the dominant summertime source of VOC reactivity even in most major North American cities. Methane oxidation is a 2× larger source of non-methane VOCs (via production of formaldehyde and methyl hydroperoxide) over North America in the model than are anthropogenic emissions. However, anthropogenic VOCs account for over half the ambient VOC loading over the majority of the region owing to their longer aggregate lifetime. Fires can be a significant VOC source episodically but are small on average. In the planetary boundary layer (PBL), the model exhibits skill in capturing observed variability in total VOC-abundance ( $R^2 = 0.36$ ) and reactivity ( $R^2 = 0.54$ ). The same is

44 not true in the free troposphere (FT), where skill is low and there is a persistent low model bias (~60%),  
45 with most (27 of 34) model VOCs underestimated by more than a factor of 2. A comparison of PBL:FT  
46 concentration ratios over the southeastern US points to a misrepresentation of PBL ventilation as a  
47 contributor to these model FT biases. We also find that a relatively small number of VOCs (acetone,  
48 methanol, ethane, acetaldehyde, formaldehyde, isoprene + oxidation products, methyl hydroperoxide)  
49 drive a large fraction of total ambient VOC reactivity and associated model biases; research to improve  
50 understanding of their budgets is thus warranted. A source tracer analysis suggests a current overestimate  
51 of biogenic sources for hydroxyacetone, methyl ethyl ketone and glyoxal, an underestimate of biogenic  
52 formic acid sources, and an underestimate of peroxyacetic acid production across biogenic and  
53 anthropogenic precursors. Future work to improve model representations of vertical transport and to  
54 address the VOC biases discussed are needed to advance predictions of ozone and SOA formation.

55

## 56 **1. Introduction**

57 Volatile organic compounds (VOCs) play a central role in atmospheric chemistry. Through their influence  
58 on the hydroxyl radical (OH), VOCs alter the lifetime of long-lived greenhouse gases (Cubasch et al.,  
59 2013), while their oxidation products such as ozone (O<sub>3</sub>) and secondary organic aerosols (SOA) degrade  
60 human and ecosystem health (EPA, 2018) and alter Earth's radiative balance (Myhre et al., 2013). There  
61 are large uncertainties associated with the emissions (Karl et al., 2018; Hatch et al., 2017; Guenther et al.,  
62 2012), chemical processing (Caravan et al., 2018; Shaw et al., 2018; Müller et al., 2016a), and sinks of  
63 atmospheric VOCs (Iavorivska et al., 2017; Nguyen et al., 2015; Wolfe et al., 2015; Karl et al., 2010). An  
64 ensemble of recent airborne campaigns over North America together afford the most expansive picture  
65 yet of the atmospheric VOC distribution over this region. Here we apply a high-resolution chemical  
66 transport model (nested GEOS-Chem CTM) with a new and highly comprehensive VOC treatment to 1)  
67 interpret that observational ensemble in terms of their constraints on the distribution, speciation, and  
68 sources of VOC-carbon and reactivity, 2) assess our current scientific ability to capture that distribution  
69 across diverse environments, and 3) identify priorities for future research and model improvements.

70 It is widely recognized that terrestrial ecosystems provide the largest source of VOCs to the global  
71 atmosphere, mainly through foliar emissions but also via microbial decomposition of organic material,  
72 with an estimated flux of 750-1000 Tg/yr (Safieddine et al., 2017; Guenther et al., 2012). Global  
73 anthropogenic VOC emissions are thought to be an order of magnitude lower (e.g., 100-160 Tg/yr  
74 (Glasius and Goldstein, 2016; Boucher et al., 2013)), and include contributions from mobile sources such  
75 as on-road vehicles and aircraft (Stettler et al., 2011; Parrish, 2006) and from stationary sources such as  
76 volatile chemical products, fuel production, distribution, and combustion, and waste treatment (McDonald  
77 et al., 2018; Warneke et al., 2014; de Gouw et al., 2012; Millet et al., 2012). Biomass burning, i.e.,  
78 combustion of any non-fossilized vegetation, leads to an estimated 60-400 Tg/yr of emitted VOCs,  
79 though with high uncertainty regarding potential unidentified and/or unmeasured pyrogenic compounds  
80 (Giglio et al., 2013; Akagi et al., 2011; Wiedinmyer et al., 2011; Andreae and Merlet, 2001). Ocean-  
81 atmosphere VOC fluxes have been investigated with a range of aircraft- and ship-based observations,  
82 remote sensing, and modeling approaches for species including isoprene and monoterpenes, other light  
83 hydrocarbons, halogenated species, and oxygenated VOCs such as methanol, acetone, formaldehyde,  
84 acetaldehyde, glyoxal, and carboxylic acids (Deventer et al., 2018; Kim et al., 2017; Mungall et al., 2017;  
85 Coburn et al., 2014; Yang et al., 2014a; Yang et al., 2014b; Beale et al., 2013; Yang et al., 2013; Fischer  
86 et al., 2012; Beale et al., 2011; Luo and Yu, 2010; Millet et al., 2010; Shaw et al., 2010; Millet et al.,  
87 2008; Read et al., 2008; Palmer and Shaw, 2005; Williams et al., 2004; Singh et al., 2003; Broadgate et  
88 al., 1997; Zhou and Mopper, 1997; Bonsang et al., 1988; Kanakidou et al., 1988). However, the

89 quantitative role of the ocean as a net global VOC source or sink remains uncertain (Carpenter et al.,  
90 2012; Read et al., 2012).

91 While there have been a large number of studies focusing on one or a small subset of VOCs (a recent  
92 Web of Science search for articles with topic terms (“volatile organic compound\*”) AND (“atmospher\*”)  
93 returned >6,800 results), there have been few integrated studies examining the overall suite of measured  
94 species and our ability to capture that ensemble behavior in current CTMs. In one example, de Gouw et  
95 al. (2005) examined the photochemical evolution of organic carbon from urban outflow in the  
96 northeastern US and found evidence for unidentified aerosol precursors. Later, Goldstein and Galbally  
97 (2007) compiled a rough estimate of the total VOC budget and argued that there is a large pool of  
98 uncharacterized organic compounds in the atmosphere. Heald et al. (2008) carried out an integrated  
99 assessment of total observed organic carbon based on available measurements to that point, and  
100 articulated a need for more routine and comprehensive VOC-carbon measurements, while Safieddine et  
101 al. (2017) recently performed the first CTM-based budget analysis of total organic carbon on a global  
102 scale.

103 Recent observational work has benefited from new tools (e.g., high-resolution time-of-flight mass  
104 spectrometry) that enable a more thorough and time-resolved characterization of VOC-carbon than was  
105 previously possible. For instance, new flux measurements have been able for the first time to characterize  
106 the two-way surface atmosphere exchange of VOC-carbon simultaneously across the entire mass  
107 spectrum (Karl et al., 2018; Millet et al., 2018; Park et al., 2013). In addition, recent studies (Isaacman-  
108 VanWertz et al., 2018; Hunter et al., 2017) combining a comprehensive suite of online instrumentation  
109 have been able to achieve organic carbon closure (to within error) in a forested environment and in a  
110 laboratory oxidation experiment, respectively.

111 The past decade has thus seen major advances in the scientific community’s ability to measure (e.g.,  
112 Glasius and Goldstein (2016)) as well as model (e.g., Safieddine et al. (2017)) atmospheric organic  
113 carbon, and in our laboratory-derived understanding of key VOC oxidation pathways (e.g., (Praske et al.,  
114 2018; Ehn et al., 2014; Crouse et al., 2013; Paulot et al., 2009b)). Over the same period, there have been  
115 a large number of airborne campaigns over North America that, together, are unprecedented in their  
116 chemical and spatial coverage for characterizing VOC distributions over this region. Here, we perform an  
117 integrated analysis of these airborne datasets based on a high-resolution chemical transport model (nested  
118 GEOS-Chem CTM). The model simulation includes the latest updates related to atmospheric VOCs (Sect.  
119 2) and provides a more comprehensive representation of atmospheric organics than has been available for  
120 prior model-measurement evaluations. We apply this updated model with the suite of airborne  
121 observations to assess present understanding of the processes driving atmospheric VOCs, identify  
122 knowledge gaps, and address priorities for future work. We focus in this paper specifically on non-  
123 methane VOCs; we exclude intermediate, semi-volatile, low-volatility, and extremely low-volatility  
124 organic compounds (IVOC, SVOC, LVOC, ELVOC) because a comparable suite of airborne  
125 observations does not exist for these. The Hunter et al. study referenced above found for a ponderosa pine  
126 forest that while S/IVOC and E/LVOC species accounted for most of the aerosol-forming material, VOCs  
127 dominated the ambient OH reactivity due to non-methane organics, and also provided the majority of the  
128 organic carbon mass (Hunter et al., 2017). Likewise, while organic aerosol formation and subsequent  
129 deposition is not counted explicitly as a VOC sink in our chemical mechanism, prior work has found this  
130 to be only a small fraction (<4%) of the gas-phase VOC budget (Safieddine et al., 2017).

131

## 132 2. Model description

133 We use the GEOS-Chem CTM (v10-01; [www.geos-chem.org](http://www.geos-chem.org)) driven by assimilated meteorological  
134 fields (Goddard Earth Observation System Forward Processing product, GEOS-FP) from the NASA  
135 Goddard Modeling and Assimilation Office (GMAO). Simulations are performed for 2013, the year in  
136 which several of the utilized aircraft campaigns took place. The GEOS-FP fields have spatial resolution of  
137  $0.25^{\circ} \times 0.3125^{\circ}$  and temporal resolution of 3-h for 3-D meteorological parameters and 1-h for surface  
138 quantities and mixing depths. The North American simulation used here is conducted within a nested  
139 framework ( $130\text{--}60^{\circ}\text{W}$ ,  $9.75\text{--}60^{\circ}\text{N}$ , 47 vertical layers) at the native GEOS-FP horizontal resolution (Kim  
140 et al., 2015), with timesteps of 5-min (transport/convection) and 10-min (emissions/chemistry) (Philip et  
141 al., 2016). Dynamic boundary conditions are obtained from a global simulation ( $4^{\circ} \times 5^{\circ}$ ) with timesteps of  
142 30-min (transport/convection) and 60-min (emissions/chemistry). The Supplement (Fig. S1, S2) shows an  
143 evaluation of these boundary conditions based on Atmospheric Tomography Mission (ATom) (Wofsy et  
144 al., 2018) ozone observation in the northern Pacific. We use the TPCORE advection algorithm (Lin and  
145 Rood, 1996), convective mass fluxes from the GEOS-FP archive (Wu et al., 2007), and the non-local  
146 boundary layer mixing scheme described by Lin and McElroy (2010).

147 A year-long nested model run for 2013 was obtained via 12 parallel month-long simulations. Each of the  
148 latter was initialized after a ~1-week nested spin-up of regridded concentration fields from a ~2-year  
149 global spin-up. We find that this procedure is sufficient to achieve dynamic steady-state for oxidant and  
150 VOC levels in the model, as species that would require longer spin-up (e.g., methane) are prescribed  
151 rather than actively simulated in this mechanism.

### 152 2.1 Chemistry

153 The chemical mechanism in this work is based on Millet et al. (2018), with the following modifications.  
154 Here we incorporate a more detailed treatment of monoterpene chemistry that is adapted from Fisher et al.  
155 (2016), along with updated photo-isomerization yields for acetaldehyde (Millet et al., 2015). Further  
156 updates are included for VOC ozonolysis (isoprene, methacrolein, and isoprene hydroxynitrate) (Marais  
157 et al., 2016), glyoxal and methyl glyoxal yields from aromatics (Fischer et al., 2014), carboxylic acid  
158 production from the hydrolysis of stabilized Criegee intermediates (Millet et al., 2015), and photolysis  
159 cross sections for methyl vinyl ketone (MVK) and methacrolein (MACR) nitrates and propanone nitrate  
160 (Paulot et al., 2009a). Finally, we apply the carbon mass tracking approach outlined in Safieddine et al.  
161 (2017) to ensure carbon closure.

### 162 2.2 Deposition

163 Physical VOC sinks in GEOS-Chem include dry deposition following the Wesely (1989) scheme as  
164 implemented by Wang et al. (1998), and wet deposition as described by Amos et al. (2012). Wet  
165 deposition assumes liquid-phase-only uptake of VOCs (except formic acid and acetic acid) with a  
166 retention efficiency of 1 in warm clouds and 0.02 in mixed clouds (Mari et al., 2000). Ice uptake of  
167 formic acid and acetic acid is included based on the Langmuir isotherm model (Paulot et al., 2011).

168 Henry's law solubility constants ( $H$  values; required for calculating dry deposition resistances, gas-phase  
169 wet deposition, and air-sea fluxes) are computed following Travis et al. (2016) and Nguyen et al. (2015)  
170 for nitric acid, hydrogen peroxide, and a suite of isoprene-derived oxygenated VOCs (isoprene hydroxyl  
171 hydroperoxides, isoprene hydroxynitrate, isoprene epoxides, MVK/MACR nitrates, propanone nitrate,  
172 glycolaldehyde, hydroxyacetone). Values for lumped  $\geq\text{C}_4$  alkyl nitrates and formaldehyde are based on  
173 Marais et al. (2016) and Jacob (2000), respectively, while those for benzene, toluene, and xylene  
174 (representing lumped C8 aromatics) are taken from Staudinger and Roberts (2001). The lumped xylene  
175 species in the model uses the mean  $H$  value from the corresponding individual C8 compounds (o-xylene,  
176 m-xylene, p-xylene, ethylbenzene). For other VOCs we use central literature values based on the Sander



177 (2015) compilation. Carboxylic acids employ an effective  $H$  value at  $pH=7$ , with lumped  $\geq C3$  acids using  
178 the median reported value for propionic acid (Nirmalakhandan and Speece, 1988).

## 179 2.3 Emissions

### 180 2.3.1 Natural emissions

181 Biogenic VOC emissions from terrestrial plants are calculated online in GEOS-Chem using the Model of  
182 Emissions of Gases and Aerosols from Nature version 2.1 (MEGAN v2.1), implemented into GEOS-  
183 Chem as described by Hu et al. (2015).

184  $NO_x$  emissions from microbial processes in soils are estimated as described in Hudman et al. (2012). The  
185 annual combined global flux of formic and acetic acids from soils estimated previously by Paulot et al.  
186 (2011) corresponds to approximately 10% of this  $NO_x$  source, and we therefore determine the  
187 formic/acetic acids soil fluxes as 5% (molar ratio) of the Hudman et al. (2012)  $NO_x$  flux.

188 Marine hydrocarbon emissions (for alkanes, alkenes, and isoprene) are estimated following Millet et al.  
189 (2015) and Paulot et al. (2011). Air-sea fluxes of oxygenated VOCs are calculated following Johnson  
190 (2010), Millet et al. (2010; 2008), and Fischer et al. (2012), with assumed fixed seawater concentrations  
191 of 15 nM (acetone), 31 nM (methanol), and 6 nM (acetaldehyde) based on compiled cruise measurements  
192 (Beale et al., 2015; Yang et al., 2014a; Yang et al., 2014b; Beale et al., 2013; Yang et al., 2013; Beale et  
193 al., 2011; Kameyama et al., 2009; Hudson et al., 2007; Marandino et al., 2005; Williams et al., 2004;  
194 Zhou and Mopper, 1997).

### 195 2.3.2 Anthropogenic emissions

196 Global anthropogenic VOC emissions in the model are from the Interpolated ACCMIP-RCP 8.5  
197 inventory for year-2013 (van Vuuren et al., 2011; Lamarque et al., 2010; Riahi et al., 2007) (with a few  
198 exceptions; see below). This inventory provides speciated emissions for  
199 alkanes/alkenes/alkynes/aromatics, and unspeciated emissions for alcohols/ $\geq C2$   
200 aldehydes/ketones/carboxylic acids. For the latter, we apply speciation factors for methanol and ethanol  
201 (0.5, 0.375, mass basis), acetaldehyde and  $\geq C3$  aldehydes (0.75, 0.25), and acetone and  $\geq C4$  ketones  
202 (0.75, 0.25) based on prior studies (Wells et al., 2012; Millet et al., 2010). Formic acid and acetic acid  
203 together are assumed to account for 75% by mass of the total ACCMIP carboxylic acid source (these in  
204 turn are partitioned with a 1:2 molar ratio), with  $\geq C3$  carboxylic acids making up the remaining 25%  
205 (Paulot et al., 2011).

206 Global anthropogenic and biofuel emissions of ethane and propane are from Xiao et al. (2008). Global  
207 formic and acetic acid emissions from animal agriculture are scaled to the corresponding ammonia source  
208 (from EDGAR v4.2 agricultural sectors 4C and 4D) following Paulot et al. (2011). We use global biofuel  
209 emissions from Yevich and Logan (2003) for emitted oxygenated VOCs not included in ACCMIP-RCP  
210 8.5 (glycolaldehyde, hydroxyl acetone, glyoxal, and methyl glyoxal). Aircraft emissions are from the  
211 AEIC inventory (Stettler et al., 2011), and global anthropogenic  $NO_x/CO/SO_2/NH_3$  emissions are from  
212 EDGAR v4.2 (European Commission (EC), 2011).

213 Over North America, emissions of inorganic species and VOCs (except ethane and propane) from  
214 anthropogenic, biofuel, and ship sources are overwritten by the hourly EPA/NEI2011 inventory (Travis et  
215 al., 2016; EPA, 2015), with annual scale factors applied to account for recent trends (e.g., the nationally  
216 aggregated 2011-2013 emission trend factor for VOCs is 0.971). Molar fluxes of formic and acetic acid  
217 over North America from these sources are estimated by scaling those of CO by  $2.1 \times 10^{-4}$  and  $4.2 \times 10^{-4}$ ,  
218 respectively (Paulot et al., 2011).

219 2.3.3 Biomass burning emissions  
220 Open fire emissions are calculated from monthly burned area and fractional fire type contributions from  
221 the fourth version of the Global Fire Emissions Database with small fires (GFED4s) (van der Werf et al.,  
222 2017) for our simulation year. We use the GFED-recommended species-specific emission factors  
223 (<http://www.globalfiredata.org/data.html>) which are based primarily on Akagi et al. (2011).

224

### 225 3. Airborne measurements of VOCs over North America

226 Figure 1 shows flight tracks for the airborne tropospheric chemistry missions that took place over North  
227 America between 2010-2014 and are used here. We have used data from intensive field campaigns using  
228 NCAR, NOAA and NASA aircraft that carried a large instrument payload to simultaneously measure  
229 many VOCs. Together, they provide a rich dataset for constraining VOC-related processes, as they  
230 feature extensive horizontal and vertical sampling throughout the North American troposphere and  
231 include a range of observing strategies such as survey transects, racetrack gradients/walls, and spirals.  
232 Table 1 summarizes the campaigns in terms of sampling time period, region, as well as aircraft platform  
233 and flight ceiling, with instrumental measurement details and references provided in Table S1. Below, we  
234 briefly introduce the overall goals and instrument payload for each campaign.

235 The Studies of Emissions and Atmospheric Composition, Clouds, and Climate Coupling by Regional  
236 Surveys (SEAC<sup>4</sup>RS 2013; Aug-Sep 2013) (Toon et al., 2016; SEAC<sup>4</sup>RS Science Team, 2013) was  
237 conducted over the southeastern US and targeted a broad range of goals including quantifying the  
238 regional distribution of anthropogenic, biomass burning, and biogenic chemicals, characterizing their re-  
239 distribution through convection, and identifying their impacts on boundary layer and upper tropospheric  
240 chemistry. The deployed NASA DC-8 aircraft has a flight ceiling of 12.5 km above sea level (ASL),  
241 enabling deep vertical profiling. The SEAC<sup>4</sup>RS VOC payload included a chemical ionization mass  
242 spectrometer using CF<sub>3</sub>O<sup>+</sup> reagent ions (CIT-CIMS (CF<sub>3</sub>O<sup>+</sup>)), a separate CIMS measuring peroxy acetyl  
243 nitrate (PAN-CIMS), a proton-transfer-reaction mass spectrometer (PTR-MS), in situ airborne  
244 formaldehyde measurements by laser induced fluorescence (ISAF-LIF), thermal dissociation LIF (TD-  
245 LIF), and a whole air sampler (WAS). Specific VOCs measured by each instrument are listed in Table S1.

246 The Southeast Nexus (SENEX; Jun 2013) campaign (Warneke et al., 2016) was part of the Southeast  
247 Atmosphere Study (SAS). The NOAA WP-3D aircraft sampled the boundary layer through mid-  
248 troposphere (up to 6.4 km ASL), targeting both natural and anthropogenic emissions. Onboard VOC  
249 instruments included WAS, ISAF-LIF, PAN-CIMS, and PTR-MS. SENEX also featured in-situ  
250 measurements of carboxylic acids by two separate CIMS using iodide reagent ions (I-CIMS) and of  
251 glyoxal via airborne cavity enhanced spectrometer (ACES) (Table S1).

252 The Deep Convective Clouds and Chemistry (DC3; May-Jun 2012) field experiments took place over the  
253 central US and were specifically designed to investigate changes in upper tropospheric composition and  
254 chemistry during and after deep convective events (Barth et al., 2015; DC3 Science Team, 2013). During  
255 DC3 the NASA DC-8 and GV aircraft sampled storm outflow up to 13 km ASL through spirals and wall  
256 sampling. The VOC payload included PTR-MS, a Trace Organic Gas Analyzer (TOGA), CIT-CIMS  
257 (CF<sub>3</sub>O<sup>+</sup>), PAN-CIMS, ISAF-LIF, TD-LIF, and WAS.

258 The California Research at the Nexus of Air Quality and Climate Change (CalNex; May-June 2010)  
259 campaign studied air quality and climate over California and offshore (Ryerson et al., 2013). The NOAA  
260 WP-3D aircraft sampled the troposphere up to 5 km ASL, and carried out survey tracks over the northern,  
261 central, and southern San Joaquin Valley and Los Angeles basin, with spirals over targeted urban and  
262 agricultural sources. VOCs were measured onboard by PTR-MS, PAN-CIMS, and WAS.

263 DISCOVER-AQ (Deriving Information on Surface Conditions from Column and Vertically Resolved  
264 Observations Relevant to Air Quality) (Crawford and Pickering, 2014; DISCOVER-AQ Science Team,  
265 2014) included four separate airborne campaigns: DISCOVER-AQ DC (Jun-Jul 2011) over Baltimore-  
266 Washington DC, DISCOVER-AQ CA (Jan-Feb 2013) over the San Joaquin Valley, DISCOVER-AQ TX  
267 (Sep 2013) over Houston, and DISCOVER-AQ CO (Jul-Aug 2014) over the Denver Colorado urban  
268 region. The NASA P3-B aircraft (8.5 km ASL ceiling) was employed in each case, with frequent and  
269 repeated spirals to characterize the vertical structure of the troposphere. The VOC payload included a  
270 difference frequency generation absorption spectrometer (DFGAS) and time-of-flight PTR-MS (PTR-  
271 ToF-MS; quadrupole PTR-MS was used for DISCOVER-AQ DC).

272 FRAPPÉ (Front Range Air Pollution and Photochemistry Experiment; Jul-Aug 2014) took place jointly  
273 with DISCOVER-AQ CO, with the employed NCAR C-130 aircraft (8 km ASL ceiling) sampling the  
274 broader mountain-plain areas over northern Colorado. The VOC payload included PTR-MS, a compact  
275 atmospheric multi-species spectrometer (CAMS), TOGA, peroxide CIMS (PCIMS), PAN-CIMS, and  
276 WAS.

277 We use 1-minute merged data from each campaign to match the frequency at which the GEOS-Chem  
278 output is sampled along the aircraft flight tracks. For species co-measured by multiple instruments during  
279 the same campaign, we select one measurement primarily based on time response ( $\leq$  1-min sampling rate  
280 preferred), while also considering data availability and nominal accuracy. For example, VOCs measured  
281 by PTR-MS, TOGA or CAMS (for ethane) take precedence over contemporaneous WAS observations  
282 due to the higher time resolution. The ISAF-LIF, DFGAS and CAMS instruments are specifically  
283 designed for formaldehyde, and we use these observations (rather than WAS, TOGA, or PTR-MS) in all  
284 cases with the exception of CalNex (where PTR-MS was the only available HCHO measurement). PTR-  
285 MS and TOGA measurements during FRAPPÉ are highly correlated but with 5-30% discrepancies across  
286 compounds (Fig. S3). We therefore repeated our main analyses using data from each instrument (see Fig.  
287 5-8 and Table S2-5), and find that the conclusions are not significantly changed. Similar sensitivity tests  
288 are done for formaldehyde, which had concurrent observations during DC3-DC-8 (DFGAS, ISAF-LIF)  
289 and during SEAC<sup>4</sup>RS (CAMS, ISAF-LIF), as well as for formic acid, which had concurrent observations  
290 during SENEX (NOAA CIMS, UW CIMS) (Fig. S4).

291 One concern when combining multiple measurements is the differing time resolution between  
292 instruments. For example, the WAS systems collect discrete samples separated by up to 10 min, while  
293 TOGA collects a 35 second integrated sample on alternate minutes. Many other instruments used here  
294 have significantly higher time resolution. To address this issue, when mapping aggregated quantities (i.e.,  
295 total VOC-carbon; Fig. 5), we consider only those datapoints with complete species coverage (no missing  
296 data within a given campaign's payload). Overall, this yields ~7000 (4500) 1-min averaged observational  
297 datapoints in the PBL (FT), distributed over ~900 (1700) ~25km model grid cells. Finally, to avoid  
298 comparing a single modeled value with multiple observations falling into the same model gridbox and  
299 timestep, all measurements and model output are averaged and gridded to unique model gridbox-timestep  
300 combinations.

301

## 302 **4. Simulated VOC budget over North America**

### 303 **4.1 Biogenic emissions dominate the VOC budget on a carbon basis**

304 Figure 2a depicts the annual VOC budget (in C units) over North America in 2013 as simulated by  
305 GEOS-Chem. A buffer of ten model grid boxes along each lateral boundary has been omitted to exclude  
306 unrealistic conditions near the edge of the nested domain. Total fluxes are indicated for each source and

307 sink term, representing the sum over all grid boxes within the plotted region. The net transport flux in/out  
308 of the domain is estimated from the accumulated product of the daily average eastward/northward wind  
309 components and VOC number density at the boundaries. In this way, we achieve regional VOC-carbon  
310 closure to within 3%.

311 We see in Fig. 2a that biogenic emissions are the dominant annual VOC-carbon source over North  
312 America, accounting for 71% (40 TgC) of the model total. Anthropogenic emissions account for 23% (13  
313 TgC), while VOC emissions from fires can be important in particular locations and seasons but are minor  
314 when integrated over the domain as a whole (3 TgC, 5%). Prior studies have estimated that biogenic VOC  
315 emissions are 10-12× larger than anthropogenic emissions on a global basis (Safieddine et al., 2017;  
316 Glasius and Goldstein, 2016; Boucher et al., 2013; Guenther et al., 2012; Goldstein and Galbally, 2007);  
317 our results for North America, while indicating a greater relative importance for anthropogenic emissions  
318 than in the global mean, still show that biogenic VOC-carbon emissions are ~3× anthropogenic sources  
319 even in this industrialized region. Finally, while methane is not considered as a VOC for the purpose of  
320 our analysis, its oxidation generates formaldehyde and methyl hydroperoxide, corresponding to a VOC  
321 source of 30 TgC/y over our North American domain. Methane oxidation is thus >2× larger as a non-  
322 methane VOC source over this region than anthropogenic emissions, though this source is diffuse and  
323 not-collocated with land-based fluxes.

324 During winter (Fig. 3a), we find in the model that anthropogenic sources account for the majority (54%)  
325 of emitted VOC-carbon over the domain as a whole; this fraction would be significantly higher if we were  
326 to exclude the US Gulf States, Mexico, and Central America where substantial biogenic emissions persist  
327 throughout the year. However, during summer the modeled domain-wide anthropogenic contribution is  
328 only 12%; then, it is only in the most polluted regions, where biogenic emissions are low, that  
329 anthropogenic emissions provide the main source of atmospheric reactive carbon.

330 Analogous sets of figures for NO<sub>x</sub> are provided in the supplement (Fig. S5, S6).

#### 331 4.2 Biogenic VOC emissions even more dominant on a reactivity basis

332 The predominance of biogenic over anthropogenic VOCs in North America is even more pronounced  
333 when we account for the chemical reactivity of the various species. A common metric for assessing this is  
334 the OH reactivity ( $\sum k_i n_i$ , where  $k_i$  and  $n_i$  are the OH reaction rate coefficient and atmospheric number  
335 density for chemical  $i$ ), which quantifies the OH loss rate associated with the ambient loadings of various  
336 species. In this paper, we use the term ‘VOC reactivity’ to refer specifically to that portion of the OH  
337 reactivity driven by VOCs. A related, emissions-focused measure is the OH reactivity flux: i.e.,  $\sum k_i F_i$ ,  
338 where  $F_i$  is the surface flux for VOC  $i$  (in molecular units). Since the reactivity flux is equivalent to a  
339 (mixing-height scaled) time-derivative of OH reactivity (Millet et al., 2018), it provides a direct measure  
340 of how a given surface flux affects ambient OH reactivity.

341 Figure 2b maps the modeled OH reactivity flux associated with biogenic, anthropogenic and pyrogenic  
342 VOC emissions. We see that biogenic sources in the model account for 95% of the annual reactivity-  
343 weighted VOC source over North America as a whole, with anthropogenic sources contributing just 3%.  
344 This biogenic predominance continues throughout the year, with biogenic VOCs making up 88% of the  
345 modeled domain-aggregated reactivity flux even during winter (though with strong spatial gradients; Fig.  
346 3b). During summer, that fraction increases to 96%.

347 There has been a substantial decrease in transportation-related VOC emissions over the past several  
348 decades in the US (McDonald et al., 2013; Parrish, 2006) (e.g., a factor of ~50-100 decrease was inferred  
349 over Los Angeles from 1960-2010 (Warneke et al., 2012)). According to current inventories (Fig. 3),  
350 anthropogenic emissions have declined to the point where biogenic emissions are the dominant

351 summertime source of VOC reactivity even in many major North American cities. Only in a small  
352 number of pollution hotspots (Fig. 3) are anthropogenic emissions the main source of VOC-related OH  
353 reactivity driving summertime production of ozone and other secondary products.

#### 354 4.3 Anthropogenic species comprise over half of the ambient VOC-carbon burden over most of North 355 America

356 Figure 4 (panels b, c, e, and f) shows the fractional contribution to the ambient near-surface VOC burden  
357 from anthropogenic and biogenic emissions. We quantify these contributions via model sensitivity tests  
358 with modified (-10%) biogenic and anthropogenic VOC emissions; the contribution from each emission  
359 category is then obtained by dividing the relative change in ambient VOC-carbon or reactivity by the  
360 relative emission perturbation. Partitioning the ambient VOC loading in this way provides an alternate  
361 framing of the VOC budget compared to the discussion above, which examined the VOC source flux  
362 magnitudes themselves.

363 While anthropogenic species make up only a small fraction of the total emitted VOC mass (~23%; Fig.  
364 2a), they account for more than half of the ambient near-surface VOC-carbon abundance over most of the  
365 North American domain (the median fraction in Fig. 4c is 57%). This is due to the longer aggregate  
366 model lifetime for anthropogenic versus biogenic VOCs: because of this, away from major biogenic  
367 source regions the ambient VOC-carbon loading predominantly reflects anthropogenic species. However,  
368 many of these areas have relatively low total VOC-carbon loading (Fig. 4a). The corollary of the above  
369 finding is that the ambient VOC-driven OH reactivity is controlled by biogenic species, and this is also  
370 apparent in Fig. 4 (panels e and f).

#### 371 4.4 Fate of reactive carbon over North America

372 The predominance of biogenic VOCs (in terms of total emitted VOC-carbon) combined with their  
373 relatively short ensemble lifetime leads to a spatial correlation between biogenic VOC emissions and total  
374 VOC sinks (e.g., over the southeastern US; Fig. 2a). Fig. 2a shows that of the 86 TgC of non-methane  
375 VOC added annually to the North American atmosphere through emissions, transport, and CH<sub>4</sub> oxidation,  
376 62 TgC (72%) is oxidized to CO+CO<sub>2</sub> in the model. If we exclude the oxidation of methane (nearly 100%  
377 of which goes on to form CO and CO<sub>2</sub>), then of the 56 TgC/y of primary VOCs emitted over North  
378 America, 32 TgC/y (57%) is ultimately oxidized to CO+CO<sub>2</sub> within the domain of Fig. 2. Oxidation of  
379 non-methane VOCs therefore provides an atmospheric CO+CO<sub>2</sub> source over this region greater than that  
380 from methane oxidation (30 TgC/y), and greater than that from direct anthropogenic CO emissions (also  
381 30 TgC/y).

382 Other removal processes include deposition (dry, 10 TgC/y; wet, 7 TgC/y) and net transport out of the  
383 domain (10 TgC/y). While global studies have found that wet deposition is a ~50% larger sink of organic  
384 carbon than is dry deposition (Safieddine et al., 2017; Kanakidou et al., 2012), the increased role for dry  
385 deposition found here is consistent with the higher continental coverage of our regional domain.

386 In the case of the VOC reactivity budget (Fig. 2b), we find in GEOS-Chem that chemical degradation is  
387 by far the largest sink (83%) of emitted reactivity, with physical removal via deposition (14%) and  
388 transport out of the domain (3%) making up the remainder.

389

### 390 **5. Observed versus predicted distribution of VOC-carbon and reactivity over North America**

391 In this section we use the aircraft campaigns described earlier to characterize the distribution of VOCs  
392 over North America, and assess the ability of the GEOS-Chem model to capture that distribution in terms  
393 of total carbon loading and associated reactivity.

394 For each campaign we use the 1-minute merge products provided by the NASA Langley Research Center  
395 (LaRC) and the NOAA Earth System Research Laboratory Chemical Science Division (ESRL CSD)  
396 (Table 1), and sample the model along the flight tracks at the time of measurement. Measurements have  
397 been filtered to remove fresh biomass burning ( $\text{CH}_3\text{CN} > 0.2$  ppbv) and pollution plumes ( $\text{NO}_2 > 4$  ppbv  
398 or  $\text{NO}_x/\text{NO}_y > 0.4$ ), and restricted to daytime measurements over continental North America. Model-  
399 measurement comparisons are performed for the planetary boundary layer (PBL, defined here as  $< 2$  km  
400 AGL) and free troposphere (FT,  $> 3$  km AGL) based on unique gridbox-timestep combinations.

401 For the purposes of model-measurement comparison we restrict the observed VOCs to those that are  
402 explicitly simulated by GEOS-Chem (Millet et al., 2018). This restricted set of VOCs nonetheless  
403 encompasses those species believed to be most important in terms of abundance and reactivity (Heald et  
404 al., 2008), and allows an apples-to-apples comparison between observations and model. For cases where  
405 multiple VOCs are measured together as a single quantity, the corresponding modeled VOCs are likewise  
406 summed. Similarly, measured VOCs are summed to match those that are lumped in the model.

407 VOC OH reactivities are calculated from the measured and simulated species concentrations and  
408 corresponding pressure- and temperature-dependent rate coefficients for reaction with OH. For species  
409 that are detected together but simulated separately, we use the modeled ratio to partition the measured  
410 sum in calculating the combined OH reactivity. For species that are lumped in the model but measured  
411 separately, we apply the bulk OH reaction rate coefficient from the model to the summed measurements.

412 In the case of C3 and C4 ketones and aldehydes, the model includes a dedicated tracer for acetone  
413 (ACET) and lumped tracers for  $\geq \text{C}_4$  ketones (MEK) and  $\geq \text{C}_3$  aldehydes (RCHO). On the other hand,  
414 these species are measured by PTR-MS as  $\Sigma(\text{acetone} + \text{propanal})$  and  $\Sigma(\text{MEK} + \text{butanal})$  and by TOGA as  
415 individual species. When analyzing the PTR-MS data we therefore partition the PTR-MS observations  
416 based on the median aldehyde:ketone ratio measured by TOGA during FRAPPÉ and DC3 (0.009 for  
417 propanal:acetone and 0.09 for butanal:MEK).

#### 418 5.1 Total observed VOC-carbon and reactivity over North America

419 Figure 5 (left panels) shows the resulting total VOC-carbon as observed over North America, which  
420 averages 27 ppbC in the PBL when considering all the aircraft campaigns as a single statistical ensemble.  
421 However, the campaigns span a range of instrumental payloads, seasons, and locations: campaigns with  
422 the most comprehensive VOC instrument payloads and that occur during summer reveal total PBL VOC  
423 loadings generally  $> 60$  ppbC, and up to 133 ppbC over the central and southeastern US. Campaigns over  
424 the northeastern and western US, with more limited VOC payloads, show PBL VOC loadings that  
425 average 20 ppbC and at times exceed 50 ppbC. Total VOC loadings in the FT (Fig. 5) drop by a factor of  
426  $\sim 3$  or more from those in the PBL across all environments, with an ensemble spatial mean of 9 ppbC.

427 The observed VOC-carbon loadings summarized above and plotted in Fig. 5 are broadly similar to those  
428 reported over the US by Heald et al. (2008) (averaging 8-84 ppbC with 83-97% in the gas-phase at 273K  
429 and 1013hPa), who synthesized the gas- and aerosol- phase organic carbon observations up to that time.  
430 However, observations over the US used in that study were primarily from ground-based campaigns. The  
431 10 airborne studies carried out since then and used here allow a more comprehensive spatial description  
432 of VOCs across the North American airshed. The combined dataset employed here also includes a  
433 number of additional multifunctional VOCs that can now be quantified thanks to measurement advances  
434 in the intervening decade (Glasius and Goldstein, 2016).

435 Figure 6 (left panels) shows the total OH reactivity arising from the set of observed VOC. The aggregated  
436 spatial mean VOC reactivity is  $2 \text{ s}^{-1}$  in the PBL, declining to  $0.13 \text{ s}^{-1}$  in the FT. Compared to the VOC-  
437 carbon loading, the reactivity has a much larger vertical falloff (10-20 $\times$  decrease from the PBL to the FT),

438 and greater spatial variability within the PBL. The observed VOC reactivity within the PBL is  
439 generally  $>6 \text{ s}^{-1}$  over the southeastern US,  $2\text{-}6 \text{ s}^{-1}$  over the northeastern US, and  $<2 \text{ s}^{-1}$  over the central and  
440 western US. The highest observed VOC reactivity ( $24 \text{ s}^{-1}$ ) over the southeastern US is comparable to  
441 ground-based measurements in that region ( $10\text{-}25 \text{ s}^{-1}$ ) during the SOAS study (Feiner et al., 2016; Kaiser  
442 et al., 2016).

443 The importance of biogenic VOCs for reactive carbon loading and, especially, reactivity in the PBL is  
444 evident in the maps shown in Fig. 5-6. For example, Fig. 6 shows sharply defined areas of elevated VOC  
445 reactivity in the PBL over the forests of the southeastern US, with strong horizontal gradients and much  
446 lower observed reactivity elsewhere. Similar patterns, though less starkly defined, are evident in the  
447 measured VOC-carbon distribution (Fig. 5). The highly reactive nature of many biogenic VOCs  
448 (especially isoprene and some of its oxidation products) explain their disproportionate impact on  
449 reactivity given their relative abundance, as well as the much larger spatial gradients for VOC reactivity  
450 than for total VOC-carbon.

### 451 5.2 Speciated drivers of ambient VOC-carbon and reactivity

452 Figures 7 and 8 show the species driving ambient VOC-carbon and reactivity as a function of their carbon  
453 oxidation state ( $OS_c$ ) and size (carbon number,  $n_c$ ) (Kroll et al., 2011). Within the PBL (Fig. 7b), we find  
454 that the total mean VOC-carbon is largely driven by small and relatively reduced VOCs (e.g., acetone,  
455 methanol and alkanes), though some more oxidized species (e.g., formic acid, methyl hydroperoxide,  
456 formaldehyde, other isoprene oxidation products) also make significant contributions. These smaller  
457 VOCs would represent an even larger portion of the total molar VOC-loading.

458 In the FT (Fig. 7a), mean abundances decline by  $\sim 2$ -fold or more for all measured VOCs relative to the  
459 PBL. Here, a few small, reduced (low- $OS_c$ ), and relatively long-lived species dominate the overall VOC-  
460 carbon loading, with acetone, methanol, and ethane ( $\tau \sim 12\text{-}50$  days at  $OH = 10^6 \text{ molecules/cm}^3$ ) together  
461 averaging 6.4 ppbC, compared to only 3.6 ppbC for the mean sum of all other observed species.

462 However, ambient OH reactivity is driven by a different set of VOCs. Figure 8 shows that within the  
463 PBL, formaldehyde ( $0.34 \text{ s}^{-1}$ ), acetaldehyde ( $0.19 \text{ s}^{-1}$ ), isoprene hydroxyhydroperoxides + epoxides ( $0.21$   
464  $\text{ s}^{-1}$ ), methylhydroperoxide ( $0.17 \text{ s}^{-1}$ ), and isoprene ( $0.11 \text{ s}^{-1}$ ) make the largest contributions to the mean  
465 observed VOC reactivity. Compared to the case for VOC-carbon loading (Fig. 7b), we see in the  
466 reactivity distribution a more prominent role for a number of higher- $n_c$  (and more reactive) compounds.

467 On average, the observed VOC reactivity is more than a factor of 10 lower in the FT than in the PBL,  
468 with formaldehyde ( $0.03 \text{ s}^{-1}$ ) and acetaldehyde ( $0.02 \text{ s}^{-1}$ ) still making the largest contributions to the total.  
469 Whereas the FT VOC-carbon loading is dominated by a few small VOCs (Fig. 7a), Figure 8a shows that  
470 the FT VOC reactivity is provided by a wider suite of species due to the offsetting effects of abundance  
471 and lifetime. In other words, we see important FT reactivity contributions (in the mean) from both highly-  
472 reactive (but low-abundance) VOCs such as isoprene, and from less-reactive (but highly-abundant) VOCs  
473 such as methanol.

### 474 5.3 Accuracy of CTM-predicted VOC-carbon and reactivity

475 Figures 5 and 6 also portray the ability of the GEOS-Chem CTM to represent the measured distribution of  
476 VOCs over North America. In the PBL, the model exhibits significant skill at capturing atmospheric  
477 variability in VOC-carbon and reactivity: spatial model-measurement  $R^2$  values are 0.36 and 0.54,  
478 respectively. The same is not true in the FT, where the model-measurement correlations are  $R^2 < 0.1$  for  
479 both VOC-carbon and VOC OH reactivity. This lack of explanatory power suggests that the primary  
480 drivers of VOC abundance and reactivity in the FT are not well-understood or represented in current  
481 models.

482 We also see in Fig. 5 and 6 that the model tends to underestimate the observed VOC-carbon and reactivity  
483 in the PBL across most of the sampled environments, with a normalized mean bias (NMB) of -37% and -  
484 34%, respectively. This corresponds to a mean reactive carbon underestimate in the PBL of 10 ppbC and  
485 a reactivity underestimate of  $0.6 \text{ s}^{-1}$ . A bias of this magnitude is equivalent to  $\sim 2\times$  the reactivity of  
486 methane (at 2ppm) or  $0.5\times$  that of CO (at 200 ppb), and is therefore important for accurately representing  
487 atmospheric OH chemistry and ozone production.

488 While on average the CTM underpredicts the abundance and reactivity of VOCs in the PBL, this is not  
489 the case everywhere. There are areas shown in Fig. 5 and 6 where the model either agrees with the  
490 observations or is too high - in particular over the northern Sacramento Valley and the southeastern US.  
491 Regarding the former, large methanol and acetaldehyde emissions from rice fields, with strong  
492 enhancements after flooding, were previously inferred based on the same CalNex observations over the  
493 Central Valley (Peischl et al., 2012; Warneke et al., 2011). Indeed, we find here a model overestimate of  
494 total VOC-carbon for this region before flooding and a low bias after flooding, suggesting that  
495 agricultural VOC emissions are not currently well-represented in the model. On the other hand, over the  
496 southeastern US, where biogenic emissions predominate and VOC loading is highest across all sampled  
497 areas, both the PBL VOC-carbon (observed mean of 48 ppbC) and VOC reactivity ( $4.5 \text{ s}^{-1}$ ) are captured  
498 by the model with low mean bias ( $<14\%$  for both).

499 In contrast to the PBL where both positive and negative model discrepancies occur, aloft in the FT the  
500 model exhibits a large negative bias for both VOC-carbon (-64%) and reactivity (-63%) that manifests  
501 essentially everywhere. Such a severe discrepancy has implications for our understanding of FT  $\text{HO}_x$   
502 cycling (Brune et al., 2018; Mao et al., 2009), ozone production at higher altitudes where its climatic  
503 effects are strongest (Apel et al., 2015; Bertram et al., 2007), and possibly, secondary organic aerosol  
504 loading (Bianchi et al., 2016; Cappa, 2016; Kirkby et al., 2016; Trostl et al., 2016; Heald et al., 2005). We  
505 explore potential causes for these observed discrepancies in Sect. 6.

506 Given the range in measurement years spanned by the aircraft measurements, we performed a set of one-  
507 month simulations spanning multiple years to assess the potential impact of interannual variability on  
508 these findings. Results (see Fig. S7 and text following) suggest that the key features of the model-  
509 measurement comparisons discussed here are robust across years.

#### 510 5.4 Key VOCs driving model biases in atmospheric VOC-carbon and reactivity

511 Figure 7b shows that the overall low model bias for VOC-carbon in the PBL manifests for 23 out of 34  
512 individual VOCs, with these exhibiting normalized biases ranging from -1% to -90% (Fig. S8b and S9b).  
513 In general, the largest absolute carbon biases are seen for the more abundant VOCs (Fig. 7b), and largest  
514 reactivity biases for the more reactive VOCs (Fig. 8b). Just two compounds (acetone and methanol)  
515 account for almost half of the mean negative VOC-carbon bias seen in the PBL (4.3 of 9 ppbC). For VOC  
516 reactivity, four compounds (methyl hydroperoxide, acetaldehyde, formaldehyde, and isoprene) together  
517 account for 70% of the mean model bias in the PBL ( $-0.34$  of  $-0.47 \text{ s}^{-1}$ ).

518 Aloft in the FT (Fig. 7a and 8a), we see appreciable relative biases manifest across nearly all model  
519 compounds (ranging from -7% to -100%; Fig. S8a and S9a), with 29 out of 34 VOCs biased low in the  
520 model by more than a factor of 2. Acetone, methanol, and ethane are predominant in driving the overall  
521 model VOC-carbon underestimate: these three species have a combined model bias of -3.3 ppbC, versus a  
522 total of only -2.1 ppbC for all other underestimated VOCs combined. Significant discrepancies in model  
523 simulated FT VOC reactivity are driven by both abundant but less reactive VOCs, and by reactive (but  
524 less abundant) VOCs, with acetaldehyde having by far the largest absolute bias overall ( $-0.015 \text{ s}^{-1}$ ).



525 The above comparisons point to research priorities for improving current model representations of  
526 atmospheric VOCs. Along with highly abundant VOCs (such as acetone, methanol, and ethane),  
527 acetaldehyde, formaldehyde, isoprene (plus its oxidation products), and methyl hydroperoxide drive a  
528 large fraction of total VOC reactivity and associated model biases. Advancing our current ability to model  
529 the sources, chemistry, and physical removal of this relatively small number of species could substantially  
530 improve predictions of VOC-carbon and reactivity distributions.

531

## 532 **6. Role of vertical transport in driving a persistent model VOC underestimate in the free** 533 **troposphere over North America**

534 In Sect. 5 we demonstrated that VOC abundance and reactivity are consistently underestimated by the  
535 model in the free troposphere across environments and compounds. Potential explanations for these  
536 missing FT VOCs include chemical effects (e.g., model biases in FT VOC production and loss rates) as  
537 well as dynamical effects (e.g., model biases in PBL-FT mixing). To help distinguish between these two,  
538 we plot in Fig. 9a the modeled versus observed mean PBL:FT ratio (mixing ratio units) for each VOC  
539 across the entire SEAC<sup>4</sup>RS campaign. We see that all data fall above the 1:1 ratio line, showing that the  
540 model is overestimating the PBL:FT ratio to a similar degree across all VOCs regardless of source,  
541 lifetime, and chemical properties. This consistency across compounds points to a misdiagnosis of PBL  
542 ventilation as a likely explanation for the persistent VOC underestimate in the FT (at least over the  
543 SEAC<sup>4</sup>RS domain), since other tenable mechanisms would not be expected to affect all VOCs in such a  
544 consistent way. In particular: i) a missing FT photochemical VOC source would not explain the PBL:FT  
545 discrepancy seen for primary VOCs; ii) a model bias in dry deposition or wet scavenging would  
546 differentially affect polar and soluble versus nonpolar and less soluble species; and iii) a model OH bias  
547 would impact reactive and longer-lived species to differing degrees. Findings similar to those shown in  
548 Fig. 9a are obtained for other campaigns over the southern and eastern US (SENEX, DISCOVER-AQ  
549 DC, DISCOVER-AQ TX) but not consistently elsewhere (DC3, DISCOVER-AQ CO, FRAPPÉ,  
550 DISCOVER-AQ CA, CalNex). Since the southeastern US is the major source of North American VOC-  
551 carbon and reactivity (Fig. 2), such a mixing bias would yield a significant model underestimate of the  
552 total amount of reactive organic carbon that is transported to the North American FT.

553 We can explore this issue further by considering a two-box model to conceptualize VOC partitioning  
554 between the PBL and FT. In that case, for an example VOC that is directly emitted and then subject to  
555 chemical loss by OH, PBL-FT mixing, and deposition (PBL only), the steady-state PBL:FT ratio would  
556 be linearly related to the OH rate coefficient  $k_{OH}$  with a slope determined by OH and by the PBL  
557 ventilation rate, and with an intercept determined by the PBL-FT mixing rates. Figure S10 shows that the  
558 same holds for secondary VOCs. While dilution with PBL and FT background air will also affect the  
559 PBL:FT ratio, its effect in this simplified framework will diminish as the extent of the domain considered  
560 increases, and for shorter-lived species.

561 Of the aircraft campaigns considered, SEAC<sup>4</sup>RS comes closest to the above approximation due to the  
562 larger spatial domain sampled by the DC8 aircraft. The modeled and observed PBL:FT ratios for this  
563 campaign are plotted in Fig. 9b as a function of  $k_{OH}$ . For both model and measurements, there is an  
564 approximately linear relationship, with the model generally capturing the observed PBL:FT vs.  $k_{OH}$  slope.  
565 However, with only a couple of exceptions (e.g., HCHO, C<sub>2</sub>H<sub>2</sub>), there is a clear offset between the two  
566 populations that manifests in a consistent way for both primary and secondary VOCs and across lifetimes.  
567 The offset persists even after correcting for a potential 40% PBL depth overestimate (Zhu et al., 2016) in  
568 the GEOS fields (Fig. S11). The same conclusions are obtained if we instead examine the PBL:(PBL+FT)  
569 or (PBL+FT):PBL ratios to minimize any potential influence from spurious ratios caused by near-

570 detection-limit VOC measurements (not shown). Overall, the above comparisons implicates PBL:FT  
571 mixing as a likely player in the pervasive model VOC biases found in the FT.

572 These findings are consistent with those of Yu et al. (2018), who diagnosed inadequate vertical transport  
573 in the current off-line configuration of the GEOS-Chem CTM. Yu et al. (2018) identified as causes i) the  
574 off-line convective transport scheme (leading to a +10% bias in modeled  $^{222}\text{Rn}$  at the surface, and a -5%  
575 bias in the upper troposphere), and ii) off-line archiving of the meteorological fields (+5% model surface  
576 bias and -20% upper troposphere bias). Fixing these issues would therefore reduce the errors found here  
577 for VOC in the free troposphere (~60% mean low bias) but worsen the aggregated model performance in  
578 the PBL (~30% mean low bias). In that case, we would likely see in the model a more consistent low  
579 VOC bias throughout the troposphere, which would then indicate errors in overall VOC emissions or  
580 other processes.

581

## 582 7. Role of biogenic versus anthropogenic sources in driving model biases for key oxygenated 583 VOCs in the North American boundary layer

584 Section 5 demonstrated the critical role that certain light OVOCs (e.g., formaldehyde, acetaldehyde,  
585 methanol, acetone, methyl hydroperoxide) play in defining atmospheric VOC-carbon loading and  
586 associated reactivity, and in driving model biases in those quantities. We see in Fig. 7 that while the  
587 GEOS-Chem model underestimates the abundance of most OVOCs in the PBL, some species are  
588 overestimated (analogous discrepancies are seen in the average vertical profiles; Fig. S12-21). We  
589 therefore investigate in this section the likely role of biogenic versus anthropogenic sources in driving the  
590 observed model biases for key OVOCs.

591 To this end, a unique pair of biogenic ( $\mathcal{B}_{OVOC}$ ) and anthropogenic ( $\mathcal{A}_{OVOC}$ ) source tracers was developed  
592 for each OVOC based on the mixing ratio difference along the flight track for that species between the  
593 model base-case and simulations with either i) all biogenic VOC emissions perturbed by 10%, or ii) all  
594 anthropogenic VOC emissions perturbed by 10% (see Sect. 4.3).  $\mathcal{B}_{OVOC}$  thus represents the integrated  
595 influence of direct biogenic emissions plus oxidation of biogenic precursors for a given OVOC along the  
596 aircraft flight track, based on the model simulation.  $\mathcal{A}_{OVOC}$  is likewise a marker for the combined  
597 influence of primary plus secondary anthropogenic sources. We find that the above tracers are best able to  
598 capture the observed in-PBL OVOC variance for the SEAC<sup>4</sup>RS, SENEX, and DISCOVER-AQ TX  
599 campaigns (Table S6), arguing that the allocation of model VOC sources has the highest spatial reliability  
600 over the southeastern US region. We therefore focus our source-tracer interpretation on these specific  
601 campaigns.

602 Figure 10 plots the model bias for select OVOCs as a function of  $\mathcal{B}_{OVOC}$  and  $\mathcal{A}_{OVOC}$ , and shows that in  
603 several cases the model OVOC errors exhibit a clear relationship with one (or both) of these source  
604 tracers. For example, the positive model bias seen previously (Fig. 7) for hydroxyacetone (HAC), methyl  
605 ethyl ketone (MEK), and glyoxal (CHOCHO) is strongly correlated with the biogenic source tracer  
606  $\mathcal{B}_{OVOC}$  for each species, with the largest model overestimates occurring when  $\mathcal{B}_{OVOC}$  is high. This points  
607 to a current model overestimate of the biogenic sources of HAC, MEK, and CHOCHO, either due to  
608 biases in their precursor emissions (e.g., (Kaiser et al., 2018; Zhu et al., 2016; Wolfe et al., 2015)) or in  
609 their chemical formation mechanisms (e.g., (Miller et al., 2017; Li et al., 2016)). Model sink errors may  
610 also play a role (e.g., (Curry et al., 2018)); however, to explain the results in Fig. 10, such biases would  
611 need to be spatially correlated with emissions.

612 Conversely, in the case of formic acid (HCOOH) the model bias becomes more negative with increasing  
613 biogenic influence (consistent results are obtained with either the UW or NOAA measurements, Fig.

614 S22), which is consistent with earlier findings (Alwe et al., 2019; Millet et al., 2015; Stavrou et al.,  
615 2012) pointing to an underestimated biogenic source of HCOOH or its precursors over the southeastern  
616 US. The negative model bias seen for PAA (Fig. 7) increases with both  $\mathcal{B}_{OVOC}$  and  $\mathcal{A}_{OVOC}$  (Fig. 10),  
617 which may indicate a generic underestimate of PAA production across biogenic and anthropogenic VOCs  
618 or an overestimation of its chemical loss.

619 Findings for other OVOCs tend to be less clear and/or less consistent across these campaigns.  
620 Acetaldehyde ( $\text{CH}_3\text{CHO}$ ) is biased low in the model, on average, across the aircraft campaigns (Fig. 7),  
621 and there is some indication that this is partly due to underrepresented anthropogenic sources (Fig. 10,  
622 S22-S24). Acetone and methanol are strongly underestimated by the model (Fig. 7), which drives a  
623 significant part of the overall model VOC-carbon bias over North America. However, Fig. 10 shows that  
624 while the model bias is negative under low values of  $\mathcal{B}_{OVOC}$ , it is positive under high values of  $\mathcal{B}_{OVOC}$   
625 (this is specifically the case for SEAC<sup>4</sup>RS and DISCOVER-AQ TX; Fig. S22-S24): this may indicate a  
626 model overestimate of direct biogenic emissions combined with an underestimate of regional background  
627 concentrations or of other sources.

628

## 629 **8. Summary**

630 We performed an integrated analysis of the atmospheric VOC budget over North America based on an  
631 ensemble of recent airborne observations interpreted with an updated version of the GEOS-Chem CTM.  
632 86 TgC of non-methane VOC is added annually to the North American atmosphere in the model through  
633 emissions (biogenic: 40 TgC; anthropogenic 13 TgC; fires: 3 TgC), and  $\text{CH}_4$  oxidation (30 TgC/y). Of  
634 that, 62 TgC is oxidized to  $\text{CO}/\text{CO}_2$ , with the rest removed by deposition (dry: 7 TgC/y; wet: 10 TgC/y)  
635 and net transport out of the domain (10 TgC/y).

636 The simulated North American VOC budget shows the dominance of biogenic VOC emissions on a  
637 carbon basis (71%) and even more markedly on a reactivity basis (95%). Anthropogenic emissions  
638 provide the dominant summertime source of VOC-carbon and reactivity only in a fairly small number of  
639 pollution hotspots, and annually is  $>2\times$  smaller as a source of non-methane VOC over North America  
640 than is methane oxidation. Nevertheless, anthropogenic VOCs provide more than half of the ambient  
641 VOC-carbon burden over the majority of the region due to their longer average lifetime relative to  
642 biogenic species.

643 While on-road VOC emissions in North America have undergone a substantial decrease in the past few  
644 decades (McDonald et al., 2013; Warneke et al., 2012), recent studies have pointed to the importance of i)  
645 emerging VOC sources from oil and gas facilities (Li et al., 2017; Pfister et al., 2017), ii) volatile  
646 chemical products (McDonald et al., 2018), and iii) unexpectedly large urban OVOC fluxes (Karl et al.,  
647 2018). It is possible that such sources are not well captured in current inventories such as those used here,  
648 which in turn could alter the budget understanding above. These areas require further research to better  
649 understand the importance of such emissions for atmospheric chemistry, and to test and improve their  
650 representation in models.

651 Based on the collective aircraft observations, we find that total ambient VOC-carbon over North America  
652 is dominated by small and relatively reduced VOCs (e.g., acetone, methanol, alkanes), along with some  
653 oxidized species (e.g., formic acid, methyl hydroperoxide, formaldehyde, other isoprene oxidation  
654 products) that are also substantial VOC-carbon reservoirs in the planetary boundary layer (PBL). In the  
655 free troposphere (FT), acetone, methanol, and ethane together average 6 ppbC over the ensemble of  
656 airborne data, compared to only 4 ppbC for the sum of all other measured VOCs. Formaldehyde and  
657 acetaldehyde provide the largest source of VOC reactivity, on average, in both the PBL and FT, with a

658 range of other reactive (but less abundant) and abundant (but less reactive) species also making  
659 significant contributions.

660 The GEOS-Chem CTM with state-of-science VOC treatment captures a significant portion of the  
661 observed ambient variability for VOC-carbon ( $R^2 = 0.36$ ) and reactivity (0.54) in the PBL, but not in the  
662 FT (0.07 and 0.04) – suggesting that the main factors influencing VOC abundances in the FT are  
663 inadequately represented in current models. The GEOS-Chem model exhibits both underestimates and  
664 overestimates of the observed VOC-carbon and reactivity in the PBL, depending on location, with an  
665 overall normalized mean bias of -37% (carbon) and -34% (reactivity). This mean bias is equivalent to  $\sim 2\times$   
666 the reactivity of methane at 2 ppm or  $0.5\times$  that of CO at 200 ppb, and is therefore important from the  
667 point of view of accurately predicting OH chemistry and ozone production.

668 In the FT, the model exhibits a persistent low bias ( $\sim 60\%$ ) for VOC-carbon and reactivity that manifests  
669 essentially everywhere. A comparison of modeled versus observed PBL:FT VOC concentration ratios  
670 over the southeastern US suggests that inadequate PBL ventilation in the model may play a role in driving  
671 the observed FT biases. Recent work has sought to improve CTM transport performance through  
672 improved spatial resolution (e.g., (Zhuang et al., 2018; Yu et al., 2016)), through use of a cubed-sphere  
673 rather than regular Cartesian grid (e.g., (Eastham et al., 2018; Yu et al., 2018)), and by integration into  
674 earth system models with online coupled meteorology (e.g., (Hu et al., 2018; Long et al., 2015)). Further  
675 work is needed to specifically assess model treatment of PBL-FT coupling (e.g., using PAN:NO<sub>x</sub> or other  
676 diagnostic quantities) and PBL depths to improve tracer simulations in the FT.

677 We used a source tracer analysis to investigate the likely role of biogenic versus anthropogenic sources in  
678 driving model biases for key oxygenated VOCs. Results point to a current overestimate of the (primary +  
679 secondary) biogenic sources of hydroxyacetone, methyl ethyl ketone, and glyoxal and an underestimate of  
680 the biogenic sources of formic acid. Results also suggest a possible underestimate of the anthropogenic  
681 sources of acetaldehyde, along with an underestimate of peroxyacetic acid production across both  
682 biogenic and anthropogenic precursors. Finally, we find that a relatively modest number of individual  
683 VOCs (acetone, methanol, ethane, acetaldehyde, formaldehyde, isoprene + oxidation products, methyl  
684 hydroperoxide) drive a significant fraction of the total ambient VOC-carbon and reactivity (and  
685 associated model biases) across many environments. These species therefore merit further research to  
686 better understand their budgets and to improve model representation of VOC chemistry and the resulting  
687 effects on SOA, O<sub>3</sub>, and other oxidants.

688

#### 689 **Data availability**

690 Aircraft data used here are available at NASA LaRC (<https://www-air.larc.nasa.gov/missions.htm>) and  
691 NOAA ESRL ESD (<https://esrl.noaa.gov/csd/field.html>). GEOS-Chem model code is available at  
692 [www.geos-chem.org](http://www.geos-chem.org).

693

#### 694 **Author contributions**

695 X. Chen, D. B. Millet, H. B. Singh, and A. Wisthaler designed the study. X. Chen and D. B. Millet led the  
696 model development, simulations, all analyses, and manuscript preparation. The following authors  
697 provided measurements used in the analysis and contributed to manuscript preparation and data  
698 interpretation: A. Wisthaler, T. Mikoviny, and M. Müller (DC3, SEAC<sup>4</sup>RS, and DISCOVER-AQ PTR-  
699 MS), E. C. Apel and H. S. Hornbrook (TOGA), E. L. Atlas (CalNex WAS), D. R. Blake (CalNex,  
700 SEAC<sup>4</sup>RS, and FRAPPÉ WAS), S. S. Brown, K.-E. Min, and R. A. Washenfelder (SENEX glyoxal), J.

701 D. Crouse (CIT-CIMS), J. A. de Gouw and C. Warneke (CalNex and SENEX PTR-MS), F. Flocke, G.  
702 G. Pfister, and S. Shertz (FRAPPÉ PTR-MS and PAN-CIMS), A. Fried, D. Richter, J. Walega, and P.  
703 Weibring (DFGAS and CAMS formaldehyde), B. G. Heikes, D. W. O'Sullivan, and V. Treadaway  
704 (PCIMS), J. A. Neuman (SENEX NOAA CIMS HCOOH), T. B. Ryerson, I. Bourgeois, J. Peischl, and C.  
705 R. Thompson (NOAA NO<sub>y</sub>O<sub>3</sub>), J. M. Roberts (CalNex and SENEX PAN), P. R. Veres (SENEX PAN),  
706 and B. Yuan (other PTR-MS data).

707

## 708 **Acknowledgements**

709 This research was supported by NASA Atmospheric Composition Campaign Data Analysis and  
710 Modelling (ACCDAM) program (Grant NNX14AP89G). Computing resources were provided by the  
711 Minnesota Supercomputing Institute (<https://www.msi.umn.edu>) at the University of Minnesota. We  
712 acknowledge the ECCAD database (<http://eccad.sedoo.fr>) for hosting emission inventories used in this  
713 work. We thank Kelley Wells, Katie Travis, Seb Eastham, Joel Thornton, Paul Wennberg, and Gao Chen  
714 for their assistance and useful discussions.

715 We thank the CalNex, DC3, SENEX, SEAC<sup>4</sup>RS, DISCOVER-AQ, and FRAPPÉ teams for making this  
716 work possible. In particular, we acknowledge the contributions of Martin Graus (SENEX PTR-MS),  
717 Jessica Gilman (SENEX WAS), Lisa Kaser (FRAPPÉ PTR-MS), Joel Thornton, Ben Lee and Felipe  
718 Lopez-Hilfiker (UW CIMS), Thomas Hanisco and Glenn Wolfe (ISAF-LIF), Ronald Cohen (TD-LIF),  
719 Greg Huey (GIT CIMS), Andrew Weinheimer and Denise Montzka (NCAR NO<sub>x</sub>/NO<sub>y</sub>), and Tara  
720 Yacovitch and Scott Herndon (DISCOVER-AQ Colorado ethane).

721 A. Wisthaler acknowledges the Austrian Federal Ministry for Transport, Innovation and Technology  
722 (bmvit) through the Austrian Space Applications Programme (ASAP) of the Austrian Research  
723 Promotion Agency (FFG) for supporting the PTR-MS measurements during DC3, SEAC<sup>4</sup>RS and  
724 DISCOVER-AQ. T. Mikoviny was supported by an appointment to the NASA Postdoctoral Program at  
725 the Langley Research Center administered by Oak Ridge Associated Universities through a contract with  
726 NASA.

727 F. Flocke and G. G. Pfister thank the State of Colorado/Colorado Department of Public Health and  
728 Environment and the National Science Foundation (NSF) for funding of FRAPPÉ. The National Center  
729 for Atmospheric Research is sponsored by NSF.

730

731 **References**

- 732 Akagi, S. K., Yokelson, R. J., Wiedinmyer, C., Alvarado, M. J., Reid, J. S., Karl, T., Crounse, J. D., and Wennberg, P. O.:  
733 Emission factors for open and domestic biomass burning for use in atmospheric models, *Atmos. Chem. Phys.*, 11, 4039-4072,  
734 <https://doi.org/10.5194/acp-11-4039-2011>, 2011.
- 735 Alwe, H. D., Millet, D. B., Chen, X., Raff, J. D., Payne, Z. C., and Fledderman, K.: Oxidation of Volatile Organic Compounds as  
736 the Major Source of Formic Acid in a Mixed Forest Canopy, *Geophys Res Lett*, 46, 2940-2948,  
737 <https://doi.org/10.1029/2018GL081526>, 2019.
- 738 Amos, H. M., Jacob, D. J., Holmes, C. D., Fisher, J. A., Wang, Q., Yantosca, R. M., Corbitt, E. S., Galarneau, E., Rutter, A. P.,  
739 Gustin, M. S., Steffen, A., Schauer, J. J., Graydon, J. A., St Louis, V. L., Talbot, R. W., Edgerton, E. S., Zhang, Y., and  
740 Sunderland, E. M.: Gas-particle partitioning of atmospheric Hg(II) and its effect on global mercury deposition, *Atmos. Chem.*  
741 *Phys.*, 12, 591-603, <https://doi.org/10.5194/acp-12-591-2012>, 2012.
- 742 Andreae, M. O., and Merlet, P.: Emission of trace gases and aerosols from biomass burning, *Global Biogeochem Cy*, 15, 955-  
743 966, <https://doi.org/10.1029/2000gb001382>, 2001.
- 744 Apel, E. C., Emmons, L. K., Karl, T., Flocke, F., Hills, A. J., Madronich, S., Lee-Taylor, J., Fried, A., Weibring, P., Walega, J.,  
745 Richter, D., Tie, X., Mauldin, L., Campos, T., Weinheimer, A., Knapp, D., Sive, B., Kleinman, L., Springston, S., Zaveri, R.,  
746 Ortega, J., Voss, P., Blake, D., Baker, A., Warneke, C., Welsh-Bon, D., de Gouw, J., Zheng, J., Zhang, R., Rudolph, J.,  
747 Junkermann, W., and Riemer, D. D.: Chemical evolution of volatile organic compounds in the outflow of the Mexico City  
748 Metropolitan area, *Atmos. Chem. Phys.*, 10, 2353-2375, <https://doi.org/10.5194/acp-10-2353-2010>, 2010.
- 749 Apel, E. C., Hornbrook, R. S., Hills, A. J., Blake, N. J., Barth, M. C., Weinheimer, A., Cantrell, C., Rutledge, S. A., Basarab, B.,  
750 Crawford, J., Diskin, G., Homeyer, C. R., Campos, T., Flocke, F., Fried, A., Blake, D. R., Brune, W., Pollack, I., Peischl, J.,  
751 Ryerson, T., Wennberg, P. O., Crounse, J. D., Wisthaler, A., Mikoviny, T., Huey, G., Heikes, B., O'Sullivan, D., and Riemer, D.  
752 D.: Upper tropospheric ozone production from lightning NO<sub>x</sub>-impacted convection: Smoke ingestion case study from the DC3  
753 campaign, *J. Geophys. Res. Atmos.*, 120, 2505-2523, <https://doi.org/10.1002/2014JD022121>, 2015.
- 754 Barth, M. C., Cantrell, C. A., Brune, W. H., Rutledge, S. A., Crawford, J. H., Huntrieser, H., Carey, L. D., MacGorman, D.,  
755 Weisman, M., Pickering, K. E., Bruning, E., Anderson, B., Apel, E., Biggerstaff, M., Campos, T., Campuzano-Jost, P., Cohen,  
756 R., Crounse, J., Day, D. A., Diskin, G., Flocke, F., Fried, A., Garland, C., Heikes, B., Honomichl, S., Hornbrook, R., Huey, L. G.,  
757 Jimenez, J. L., Lang, T., Lichtenstern, M., Mikoviny, T., Nault, B., O'Sullivan, D., Pan, L. L., Peischl, J., Pollack, I., Richter, D.,  
758 Riemer, D., Ryerson, T., Schlager, H., St Clair, J., Walega, J., Weibring, P., Weinheimer, A., Wennberg, P., Wisthaler, A.,  
759 Wooldridge, P. J., and Ziegler, C.: The Deep Convective Clouds and Chemistry (DC3) Field Campaign, *B Am Meteorol Soc*, 96,  
760 1281-1309, <https://doi.org/10.1175/Bams-D-13-00290.1>, 2015.
- 761 Beale, R., Liss, P. S., Dixon, J. L., and Nightingale, P. D.: Quantification of oxygenated volatile organic compounds in seawater  
762 by membrane inlet-proton transfer reaction/mass spectrometry, *Anal. Chim. Acta*, 706, 128-134,  
763 <https://doi.org/10.1016/j.aca.2011.08.023>, 2011.
- 764 Beale, R., Dixon, J. L., Arnold, S. R., Liss, P. S., and Nightingale, P. D.: Methanol, acetaldehyde, and acetone in the surface  
765 waters of the Atlantic Ocean, *J. Geophys. Res. Oceans*, 118, 5412-5425, <https://doi.org/10.1002/jgrc.20322>, 2013.
- 766 Beale, R., Dixon, J. L., Smyth, T. J., and Nightingale, P. D.: Annual study of oxygenated volatile organic compounds in UK shelf  
767 waters, *Mar. Chem.*, 171, 96-106, <https://doi.org/10.1016/j.marchem.2015.02.013>, 2015.
- 768 Bertram, T. H., Perring, A. E., Wooldridge, P. J., Crounse, J. D., Kwan, A. J., Wennberg, P. O., Scheuer, E., Dibb, J., Avery, M.,  
769 Sachse, G., Vay, S. A., Crawford, J. H., McNaughton, C. S., Clarke, A., Pickering, K. E., Fuelberg, H., Huey, G., Blake, D. R.,  
770 Singh, H. B., Hall, S. R., Shetter, R. E., Fried, A., Heikes, B. G., and Cohen, R. C.: Direct measurements of the convective  
771 recycling of the upper troposphere, *Science*, 315, 816-820, <https://doi.org/10.1126/science.1134548>, 2007.
- 772 Bianchi, F., Trostl, J., Junninen, H., Frege, C., Henne, S., Hoyle, C. R., Molteni, U., Herrmann, E., Adamov, A., Bukowiecki, N.,  
773 Chen, X., Duplissy, J., Gysel, M., Hutterli, M., Kangasluoma, J., Kontkanen, J., Kurten, A., Manninen, H. E., Munch, S.,  
774 Perakyla, O., Petaja, T., Rondo, L., Williamson, C., Weingartner, E., Curtius, J., Worsnop, D. R., Kulmala, M., Dommen, J., and  
775 Baltensperger, U.: New particle formation in the free troposphere: A question of chemistry and timing, *Science*, 352, 1109-1112,  
776 <https://doi.org/10.1126/science.aad5456>, 2016.

- 777 Blake, N. J., Blake, D. R., Swanson, A. L., Atlas, E., Flocke, F., and Rowland, F. S.: Latitudinal, vertical, and seasonal variations  
778 of C1-C4 alkyl nitrates in the troposphere over the Pacific Ocean during PEM-Tropics A and B: Oceanic and continental sources,  
779 *J. Geophys. Res. Atmos.*, 108, <https://doi.org/10.1029/2001jd001444>, 2003.
- 780 Bonsang, B., Kanakidou, M., Lambert, G., and Monfray, P.: The marine source of C2-C6 aliphatic-hydrocarbons, *J. Atmos.*  
781 *Chem.*, 6, 3-20, <https://doi.org/10.1007/Bf00048328>, 1988.
- 782 Boucher, O., Randall, D., Artaxo, P., Bretherton, C., Feingold, G., Forster, C., Kerminen, V. M., Kondo, Y., Liao, H., Lohmann,  
783 U., Rasch, P., Satheesh, S. K., Sherwood, S., and Stevens, B.: Clouds and aerosols, in: *Climate Change 2013: The Physical*  
784 *Science Basis. Contribution of Working Group I to the Fifth Assessment Report of the Intergovernmental Panel on Climate*  
785 *Change*, edited by: Stocker, T. F., Qin, D., Plattner, G.-K., Tignor, M., Allen, S. K., Boschung, J., Nauels, A., Xia, Y., Bex, V.,  
786 and Midgley, P. M., Cambridge University Press, Cambridge, United Kingdom and New York, NY, USA, 571–658, 2013.
- 787 Broadgate, W. J., Liss, P. S., and Penkett, S. A.: Seasonal emissions of isoprene and other reactive hydrocarbon gases from the  
788 ocean, *Geophys Res Lett*, 24, 2675-2678, <https://doi.org/10.1029/97gl02736>, 1997.
- 789 Brune, W. H., Ren, X. R., Zhang, L., Mao, J. Q., Miller, D. O., Anderson, B. E., Blake, D. R., Cohen, R. C., Diskin, G. S., Hall,  
790 S. R., Hanisco, T. F., Huey, L. G., Nault, B. A., Peisch, J., Pollack, I., Ryerson, T. B., Shingler, T., Sorooshian, A., Ullmann, K.,  
791 Wisthaler, A., and Wooldridge, P. J.: Atmospheric oxidation in the presence of clouds during the Deep Convective Clouds and  
792 Chemistry (DC3) study, *Atmos. Chem. Phys.*, 18, 14493-14510, <https://doi.org/10.5194/acp-18-14493-2018>, 2018.
- 793 Cappa, C.: Atmospheric science: Unexpected player in particle formation, *Nature*, 533, 478-479,  
794 <https://doi.org/10.1038/533478a>, 2016.
- 795 Caravan, R. L., Khan, M. A. H., Zador, J., Sheps, L., Antonov, I. O., Rotavera, B., Ramasesha, K., Au, K., Chen, M. W., Rosch,  
796 D., Osborn, D. L., Fittschen, C., Schoemaeker, C., Duncianu, M., Grira, A., Dusanter, S., Tomas, A., Percival, C. J., Shallcross,  
797 D. E., and Taatjes, C. A.: The reaction of hydroxyl and methylperoxy radicals is not a major source of atmospheric methanol,  
798 *Nat. Commun.*, 9, 4343, <https://doi.org/10.1038/s41467-018-06716-x>, 2018.
- 799 Carpenter, L. J., Archer, S. D., and Beale, R.: Ocean-atmosphere trace gas exchange, *Chem. Soc. Rev.*, 41, 6473-6506,  
800 <https://doi.org/10.1039/c2cs35121h>, 2012.
- 801 Cazorla, M., Wolfe, G. M., Bailey, S. A., Swanson, A. K., Arkinson, H. L., and Hanisco, T. F.: A new airborne laser-induced  
802 fluorescence instrument for in situ detection of formaldehyde throughout the troposphere and lower stratosphere, *Atmos. Meas.*  
803 *Tech.*, 8, 541-552, <https://doi.org/10.5194/amt-8-541-2015>, 2015.
- 804 Coburn, S., Ortega, I., Thalman, R., Blomquist, B., Fairall, C. W., and Volkamer, R.: Measurements of diurnal variations and  
805 eddy covariance (EC) fluxes of glyoxal in the tropical marine boundary layer: description of the Fast LED-CE-DOAS instrument,  
806 *Atmos. Meas. Tech.*, 7, 3579-3595, <https://doi.org/10.5194/amt-7-3579-2014>, 2014.
- 807 Colman, J. J., Swanson, A. L., Meinardi, S., Sive, B. C., Blake, D. R., and Rowland, F. S.: Description of the analysis of a wide  
808 range of volatile organic compounds in whole air samples collected during PEM-tropics A and B, *Anal. Chem.*, 73, 3723-3731,  
809 <https://doi.org/10.1021/ac010027g>, 2001.
- 810 Crawford, J. H., and Pickering, K. E.: Advancing Strategies for Air Quality Observations in the Next Decade, *Environ. Manage.*,  
811 4-7, 2014.
- 812 Crounse, J. D., McKinney, K. A., Kwan, A. J., and Wennberg, P. O.: Measurement of gas-phase hydroperoxides by chemical  
813 ionization mass spectrometry, *Anal. Chem.*, 78, 6726-6732, <https://doi.org/10.1021/ac0604235>, 2006.
- 814 Crounse, J. D., Nielsen, L. B., Jørgensen, S., Kjaergaard, H. G., and Wennberg, P. O.: Autoxidation of Organic Compounds in  
815 the Atmosphere, *J. Phys. Chem. Lett.*, 4, 3513-3520, <https://doi.org/10.1021/jz4019207>, 2013.
- 816 Cubasch, U., Wuebbles, D., Chen, D., Facchini, M. C., Frame, C. L., Mahowald, N., and Winther, J.-G.: Introduction, in: *Climate*  
817 *Change 2013: The Physical Science Basis. Contribution of Working Group I to the Fifth Assessment Report of the*  
818 *Intergovernmental Panel on Climate Change*, edited by: Stocker, T. F., Qin, D., Plattner, G.-K., Tignor, M., Allen, S. K.,  
819 Boschung, J., Nauels, A., Xia, Y., Bex, V., and Midgley, P. M., Cambridge University Press, Cambridge, United Kingdom and  
820 New York, NY, USA, 119–158, 2013.

821 Curry, L. A., Tsui, W. G., and McNeill, V. F.: Technical note: Updated parameterization of the reactive uptake of glyoxal and  
822 methylglyoxal by atmospheric aerosols and cloud droplets, *Atmos. Chem. Phys.*, 18, 9823-9830, [https://doi.org/10.5194/acp-18-](https://doi.org/10.5194/acp-18-9823-2018)  
823 9823-2018, 2018.

824 DC3 Science Team: DC3 Field Campaign Data from DC-8 aircraft. NASA Langley Atmospheric Science Data Center DAAC,  
825 <https://doi.org/10.5067/aircraft/dc3/dc8/aerosol-tracegas>, 2013.

826 de Gouw, J., and Warneke, C.: Measurements of volatile organic compounds in the earth's atmosphere using proton-transfer-  
827 reaction mass spectrometry, *Mass Spectrom. Rev.*, 26, 223-257, <https://doi.org/10.1002/mas.20119>, 2007.

828 de Gouw, J. A., Middlebrook, A. M., Warneke, C., Goldan, P. D., Kuster, W. C., Roberts, J. M., Fehsenfeld, F. C., Worsnop, D.  
829 R., Canagaratna, M. R., Pszenny, A. A. P., Keene, W. C., Marchewka, M., Bertman, S. B., and Bates, T. S.: Budget of organic  
830 carbon in a polluted atmosphere: Results from the New England Air Quality Study in 2002, *J. Geophys. Res. Atmos.*, 110,  
831 <https://doi.org/10.1029/2004jd005623>, 2005.

832 de Gouw, J. A., Gilman, J. B., Borbon, A., Warneke, C., Kuster, W. C., Goldan, P. D., Holloway, J. S., Peischl, J., Ryerson, T.  
833 B., Parrish, D. D., Gentner, D. R., Goldstein, A. H., and Harley, R. A.: Increasing atmospheric burden of ethanol in the United  
834 States, *Geophys Res Lett*, 39, <https://doi.org/10.1029/2012gl052109>, 2012.

835 Deventer, M. J., Jiao, Y., Knox, H., Anderson, F., Ferner, M. C., Lewis, J. A., and Rhew, R. C.: Ecosystem-scale measurements  
836 of methyl halide fluxes from a brackish tidal marsh invaded with perennial pepperweed (*lepidium latifolium*), *J. Geophys. Res.*  
837 *Biogeosci.*, 123, 2104-2120, <https://doi.org/10.1029/2018JG004536>, 2018.

838 DiGangi, J. P., Boyle, E. S., Karl, T., Harley, P., Turnipseed, A., Kim, S., Cantrell, C., Maudlin, R. L., Zheng, W., Flocke, F.,  
839 Hall, S. R., Ullmann, K., Nakashima, Y., Paul, J. B., Wolfe, G. M., Desai, A. R., Kajii, Y., Guenther, A., and Keutsch, F. N.:  
840 First direct measurements of formaldehyde flux via eddy covariance: implications for missing in-canopy formaldehyde sources,  
841 *Atmos. Chem. Phys.*, 11, 10565-10578, <https://doi.org/10.5194/acp-11-10565-2011>, 2011.

842 DISCOVER-AQ Science Team: DISCOVER-AQ P-3B Aircraft In-situ Trace Gas Measurements. NASA Langley Atmospheric  
843 Science Data Center DAAC, <https://doi.org/10.5067/aircraft/discover-aq/aerosol-tracegas>, 2014.

844 Eastham, S. D., Long, M. S., Keller, C. A., Lundgren, E., Yantosca, R. M., Zhuang, J. W., Li, C., Lee, C. J., Yannetti, M., Auer,  
845 B. M., Clune, T. L., Kouatchou, J., Putman, W. M., Thompson, M. A., Trayanov, A. L., Molod, A. M., Martin, R. V., and Jacob,  
846 D. J.: GEOS-Chem High Performance (GCHP v11-02c): a next-generation implementation of the GEOS-Chem chemical  
847 transport model for massively parallel applications, *Geosci Model Dev*, 11, 2941-2953, [https://doi.org/10.5194/gmd-11-2941-](https://doi.org/10.5194/gmd-11-2941-2018)  
848 2018, 2018.

849 Ehn, M., Thornton, J. A., Kleist, E., Sipila, M., Junninen, H., Pullinen, I., Springer, M., Rubach, F., Tillmann, R., Lee, B., Lopez-  
850 Hilfiker, F., Andres, S., Acir, I. H., Rissanen, M., Jokinen, T., Schobesberger, S., Kangasluoma, J., Kontkanen, J., Nieminen, T.,  
851 Kurten, T., Nielsen, L. B., Jorgensen, S., Kjaergaard, H. G., Canagaratna, M., Maso, M. D., Berndt, T., Petaja, T., Wahner, A.,  
852 Kerminen, V. M., Kulmala, M., Worsnop, D. R., Wildt, J., and Mentel, T. F.: A large source of low-volatility secondary organic  
853 aerosol, *Nature*, 506, 476-479, <https://doi.org/10.1038/nature13032>, 2014.

854 EPA: 2011 National Emissions Inventory Data & Documentation, available at: [https://www.epa.gov/air-emissions-](https://www.epa.gov/air-emissions-inventories/2011-national-emission-inventory-nei-report)  
855 [inventories/2011-national-emission-inventory-nei-report](https://www.epa.gov/air-emissions-inventories/2011-national-emission-inventory-nei-report), last access: 8 Feb 2018, 2015.

856 EPA: Technical Support Document EPA's 2014 National Air Toxics Assessment, available at:  
857 [https://www.epa.gov/sites/production/files/2018-09/documents/2014\\_nata\\_technical\\_support\\_document.pdf](https://www.epa.gov/sites/production/files/2018-09/documents/2014_nata_technical_support_document.pdf) last access: 25 Sep  
858 2018, 2018.

859 European Commission (EC): Joint Research Centre (JRC)/Netherlands Environmental Assessment Agency (PBL), Emission  
860 Database for Global Atmospheric Research (EDGAR), release version 4.2. <http://edgar.jrc.ec.europa.eu>, 2011.

861 Feiner, P. A., Brune, W. H., Miller, D. O., Zhang, L., Cohen, R. C., Romer, P. S., Goldstein, A. H., Keutsch, F. N., Skog, K. M.,  
862 Wennberg, P. O., Nguyen, T. B., Teng, A. P., DeGouw, J., Koss, A., Wild, R. J., Brown, S. S., Guenther, A., Edgerton, E.,  
863 Baumann, K., and Fry, J. L.: Testing atmospheric oxidation in an Alabama forest, *J Atmos Sci*, 73, 4699-4710,  
864 <https://doi.org/10.1175/Jas-D-16-0044.1>, 2016.

865 Fischer, E. V., Jacob, D. J., Millet, D. B., Yantosca, R. M., and Mao, J.: The role of the ocean in the global atmospheric budget of  
866 acetone, *Geophys Res Lett*, 39, n/a-n/a, <https://doi.org/10.1029/2011gl050086>, 2012.



- 867 Fischer, E. V., Jacob, D. J., Yantosca, R. M., Sulprizio, M. P., Millet, D. B., Mao, J., Paulot, F., Singh, H. B., Roiger, A., Ries,  
868 L., Talbot, R. W., Dzepina, K., and Deolal, S. P.: Atmospheric peroxyacetyl nitrate (PAN): a global budget and source  
869 attribution, *Atmos. Chem. Phys.*, 14, 2679-2698, <https://doi.org/10.5194/acp-14-2679-2014>, 2014.
- 870 Fisher, J. A., Jacob, D. J., Travis, K. R., Kim, P. S., Marais, E. A., Miller, C. C., Yu, K., Zhu, L., Yantosca, R. M., Sulprizio, M.  
871 P., Mao, J., Wennberg, P. O., Crouse, J. D., Teng, A. P., Nguyen, T. B., St Clair, J. M., Cohen, R. C., Romer, P., Nault, B. A.,  
872 Wooldridge, P. J., Jimenez, J. L., Campuzano-Jost, P., Day, D. A., Hu, W., Shepson, P. B., Xiong, F., Blake, D. R., Goldstein, A.  
873 H., Misztal, P. K., Hanisco, T. F., Wolfe, G. M., Ryerson, T. B., Wisthaler, A., and Mikoviny, T.: Organic nitrate chemistry and  
874 its implications for nitrogen budgets in an isoprene- and monoterpene-rich atmosphere: constraints from aircraft (SEAC(4)RS)  
875 and ground-based (SOAS) observations in the Southeast US, *Atmos. Chem. Phys.*, 16, 5969-5991, <https://doi.org/10.5194/acp-16-5969-2016>, 2016.
- 877 Fried, A., Cantrell, C., Olson, J., Crawford, J. H., Weibring, P., Walega, J., Richter, D., Junkermann, W., Volkamer, R., Sinreich,  
878 R., Heikes, B. G., O'Sullivan, D., Blake, D. R., Blake, N., Meinardi, S., Apel, E., Weinheimer, A., Knapp, D., Perring, A., Cohen,  
879 R. C., Fuelberg, H., Shetter, R. E., Hall, S. R., Ullmann, K., Brune, W. H., Mao, J., Ren, X., Huey, L. G., Singh, H. B., Hair, J.  
880 W., Riemer, D., Diskin, G., and Sachse, G.: Detailed comparisons of airborne formaldehyde measurements with box models  
881 during the 2006 INTEX-B and MILAGRO campaigns: potential evidence for significant impacts of unmeasured and multi-  
882 generation volatile organic carbon compounds, *Atmos. Chem. Phys.*, 11, 11867-11894, <https://doi.org/10.5194/acp-11-11867-2011>, 2011.
- 884 Giglio, L., Randerson, J. T., and van der Werf, G. R.: Analysis of daily, monthly, and annual burned area using the fourth-  
885 generation global fire emissions database (GFED4), *J. Geophys. Res. Biogeosci.*, 118, 317-328,  
886 <https://doi.org/10.1002/jgrg.20042>, 2013.
- 887 Gilman, J. B., Kuster, W. C., Goldan, P. D., Herndon, S. C., Zahniser, M. S., Tucker, S. C., Brewer, W. A., Lerner, B. M.,  
888 Williams, E. J., Harley, R. A., Fehsenfeld, F. C., Warneke, C., and de Gouw, J. A.: Measurements of volatile organic compounds  
889 during the 2006 TexAQ/GoMACCS campaign: Industrial influences, regional characteristics, and diurnal dependencies of the  
890 OH reactivity, *J. Geophys. Res. Atmos.*, 114, <https://doi.org/10.1029/2008jd011525>, 2009.
- 891 Glasius, M., and Goldstein, A. H.: Recent discoveries and future challenges in atmospheric organic chemistry, *Environ. Sci.*  
892 *Technol.*, 50, 2754-2764, <https://doi.org/10.1021/acs.est.5b05105>, 2016.
- 893 Goldstein, A. H., and Galbally, I. E.: Known and unexplored organic constituents in the earth's atmosphere, *Environ. Sci.*  
894 *Technol.*, 41, 1514-1521, <https://doi.org/10.1021/Es072476p>, 2007.
- 895 Guenther, A. B., Jiang, X., Heald, C. L., Sakulyanontvittaya, T., Duhl, T., Emmons, L. K., and Wang, X.: The Model of  
896 Emissions of Gases and Aerosols from Nature version 2.1 (MEGAN2.1): an extended and updated framework for modeling  
897 biogenic emissions, *Geosci Model Dev*, 5, 1471-1492, <https://doi.org/10.5194/gmd-5-1471-2012>, 2012.
- 898 Hatch, L. E., Yokelson, R. J., Stockwell, C. E., Veres, P. R., Simpson, I. J., Blake, D. R., Orlando, J. J., and Barsanti, K. C.:  
899 Multi-instrument comparison and compilation of non-methane organic gas emissions from biomass burning and implications for  
900 smoke-derived secondary organic aerosol precursors, *Atmos. Chem. Phys.*, 17, 1471-1489, <https://doi.org/10.5194/acp-17-1471-2017>, 2017.
- 902 Heald, C. L., Jacob, D. J., Park, R. J., Russell, L. M., Huebert, B. J., Seinfeld, J. H., Liao, H., and Weber, R. J.: A large organic  
903 aerosol source in the free troposphere missing from current models, *Geophys Res Lett*, 32, n/a-n/a,  
904 <https://doi.org/10.1029/2005gl023831>, 2005.
- 905 Heald, C. L., Goldstein, A. H., Allan, J. D., Aiken, A. C., Apel, E., Atlas, E. L., Baker, A. K., Bates, T. S., Beyersdorf, A. J.,  
906 Blake, D. R., Campos, T., Coe, H., Crouse, J. D., DeCarlo, P. F., de Gouw, J. A., Dunlea, E. J., Flocke, F. M., Fried, A., Goldan,  
907 P., Griffin, R. J., Herndon, S. C., Holloway, J. S., Holzinger, R., Jimenez, J. L., Junkermann, W., Kuster, W. C., Lewis, A. C.,  
908 Meinardi, S., Millet, D. B., Onasch, T., Polidori, A., Quinn, P. K., Riemer, D. D., Roberts, J. M., Salcedo, D., Sive, B., Swanson,  
909 A. L., Talbot, R., Warneke, C., Weber, R. J., Weibring, P., Wennberg, P. O., Worsnop, D. R., Wittig, A. E., Zhang, R., Zheng, J.,  
910 and Zheng, W.: Total observed organic carbon (TOOC) in the atmosphere: a synthesis of North American observations, *Atmos.*  
911 *Chem. Phys.*, 8, 2007-2025, <https://doi.org/10.5194/acp-8-2007-2008>, 2008.
- 912 Hottle, J. R., Huisman, A. J., DiGangi, J. P., Kammrath, A., Galloway, M. M., Coens, K. L., and Keutsch, F. N.: A laser induced  
913 fluorescence-based instrument for in-situ measurements of atmospheric formaldehyde, *Environ. Sci. Technol.*, 43, 790-795,  
914 <https://doi.org/10.1021/es801621f>, 2009.

- 915 Hu, L., Millet, D. B., Baasandorj, M., Griffis, T. J., Turner, P., Helmig, D., Curtis, A. J., and Hueber, J.: Isoprene emissions and  
916 impacts over an ecological transition region in the US Upper Midwest inferred from tall tower measurements, *J. Geophys. Res.*  
917 *Atmos.*, 120, 3553-3571, <https://doi.org/10.1002/2014JD022732>, 2015.
- 918 Hu, L., Keller, C. A., Long, M. S., Sherwen, T., Auer, B., Da Silva, A., Nielsen, J. E., Pawson, S., Thompson, M. A., Trayanov,  
919 A. L., Travis, K. R., Grange, S. K., Evans, M. J., and Jacob, D. J.: Global simulation of tropospheric chemistry at 12.5 km  
920 resolution: performance and evaluation of the GEOS-Chem chemical module (v10-1) within the NASA GEOS Earth system  
921 model (GEOS-5 ESM), *Geosci Model Dev*, 11, 4603-4620, <https://doi.org/10.5194/gmd-11-4603-2018>, 2018.
- 922 Hudman, R. C., Moore, N. E., Mebust, A. K., Martin, R. V., Russell, A. R., Valin, L. C., and Cohen, R. C.: Steps towards a  
923 mechanistic model of global soil nitric oxide emissions: implementation and space based-constraints, *Atmos. Chem. Phys.*, 12,  
924 7779-7795, <https://doi.org/10.5194/acp-12-7779-2012>, 2012.
- 925 Hudson, E. D., Okuda, K., and Ariya, P. A.: Determination of acetone in seawater using derivatization solid-phase  
926 microextraction, *Anal. Bioanal. Chem.*, 388, 1275-1282, <https://doi.org/10.1007/s00216-007-1324-x>, 2007.
- 927 Huey, L. G.: Measurement of trace atmospheric species by chemical ionization mass spectrometry: speciation of reactive  
928 nitrogen and future directions, *Mass Spectrom. Rev.*, 26, 166-184, <https://doi.org/10.1002/mas.20118>, 2007.
- 929 Hunter, J. F., Day, D. A., Palm, B. B., Yatavelli, R. L. N., Chan, A. H., Kaser, L., Cappellin, L., Hayes, P. L., Cross, E. S.,  
930 Carrasquillo, A. J., Campuzano-Jost, P., Stark, H., Zhao, Y. L., Hohaus, T., Smith, J. N., Hansel, A., Karl, T., Goldstein, A. H.,  
931 Guenther, A., Worsnop, D. R., Thornton, J. A., Heald, C. L., Jimenez, J. L., and Kroll, J. H.: Comprehensive characterization of  
932 atmospheric organic carbon at a forested site, *Nat Geosci*, 10, 748+, <https://doi.org/10.1038/NGEO3018>, 2017.
- 933 Iavorivska, L., Boyer, E. W., and Grimm, J. W.: Wet atmospheric deposition of organic carbon: An underreported source of  
934 carbon to watersheds in the northeastern United States, *J. Geophys. Res. Atmos.*, 122, 3104-3115,  
935 <https://doi.org/10.1002/2016JD026027>, 2017.
- 936 Isaacman-VanWertz, G., Massoli, P., O'Brien, R., Lim, C., Franklin, J. P., Moss, J. A., Hunter, J. F., Nowak, J. B., Canagaratna,  
937 M. R., Misztal, P. K., Arata, C., Roscioli, J. R., Herndon, S. T., Onasch, T. B., Lambe, A. T., Jayne, J. T., Su, L., Knopf, D. A.,  
938 Goldstein, A. H., Worsnop, D. R., and Kroll, J. H.: Chemical evolution of atmospheric organic carbon over multiple generations  
939 of oxidation, *Nat. Chem.*, 10, 462-468, <https://doi.org/10.1038/s41557-018-0002-2>, 2018.
- 940 Jacob, D. J.: Heterogeneous chemistry and tropospheric ozone, *Atmos. Environ.*, 34, 2131-2159, [https://doi.org/10.1016/S1352-2310\(99\)00462-8](https://doi.org/10.1016/S1352-2310(99)00462-8), 2000.
- 942 Johnson, M. T.: A numerical scheme to calculate temperature and salinity dependent air-water transfer velocities for any gas,  
943 *Ocean Sci.*, 6, 913-932, <https://doi.org/10.5194/os-6-913-2010>, 2010.
- 944 Kaiser, J., Skog, K. M., Baumann, K., Bertman, S. B., Brown, S. B., Brune, W. H., Crouse, J. D., de Gouw, J. A., Edgerton, E.  
945 S., Feiner, P. A., Goldstein, A. H., Koss, A., Misztal, P. K., Nguyen, T. B., Olson, K. F., St Clair, J. M., Teng, A. P., Toma, S.,  
946 Wennberg, P. O., Wild, R. J., Zhang, L., and Keutsch, F. N.: Speciation of OH reactivity above the canopy of an isoprene-  
947 dominated forest, *Atmos. Chem. Phys.*, 16, 9349-9359, <https://doi.org/10.5194/acp-16-9349-2016>, 2016.
- 948 Kaiser, J., Jacob, D. J., Zhu, L., Travis, K. R., Fisher, J. A., Abad, G. G., Zhang, L., Zhang, X. S., Fried, A., Crouse, J. D., St  
949 Clair, J. M., and Wisthaler, A.: High-resolution inversion of OMI formaldehyde columns to quantify isoprene emission on  
950 ecosystem-relevant scales: application to the southeast US, *Atmos. Chem. Phys.*, 18, 5483-5497, <https://doi.org/10.5194/acp-18-5483-2018>, 2018.
- 952 Kameyama, S., Tanimoto, H., Inomata, S., Tsunogai, U., Ooki, A., Yokouchi, Y., Takeda, S., Obata, H., and Uematsu, M.:  
953 Equilibrator inlet-proton transfer reaction-mass spectrometry (EI-PTR-MS) for sensitive, high-resolution measurement of  
954 dimethyl sulfide dissolved in seawater, *Anal. Chem.*, 81, 9021-9026, <https://doi.org/10.1021/ac901630h>, 2009.
- 955 Kanakidou, M., Bonsang, B., Leroulet, J. C., Lambert, G., Martin, D., and Sennequier, G.: Marine source of atmospheric  
956 acetylene, *Nature*, 333, 51-52, <https://doi.org/10.1038/333051a0>, 1988.
- 957 Kanakidou, M., Duce, R. A., Prospero, J. M., Baker, A. R., Benitez-Nelson, C., Dentener, F. J., Hunter, K. A., Liss, P. S.,  
958 Mahowald, N., Okin, G. S., Sarin, M., Tsigaridis, K., Uematsu, M., Zamora, L. M., and Zhu, T.: Atmospheric fluxes of organic N  
959 and P to the global ocean, *Global Biogeochem Cy*, 26, <https://doi.org/10.1029/2011gb004277>, 2012.

- 960 Karl, T., Harley, P., Emmons, L., Thornton, B., Guenther, A., Basu, C., Turnipseed, A., and Jardine, K.: Efficient atmospheric  
961 cleansing of oxidized organic trace gases by vegetation, *Science*, 330, 816-819, <https://doi.org/10.1126/science.1192534>, 2010.
- 962 Karl, T., Striednig, M., Graus, M., Hammerle, A., and Wohlfahrt, G.: Urban flux measurements reveal a large pool of oxygenated  
963 volatile organic compound emissions, *Proc. Natl. Acad. Sci. U.S.A.*, 115, 1186-1191, <https://doi.org/10.1073/pnas.1714715115>,  
964 2018.
- 965 Kaser, L., Karl, T., Schnitzhofer, R., Graus, M., Herdinger-Blatt, I. S., DiGangi, J. P., Sive, B., Turnipseed, A., Hornbrook, R.  
966 S., Zheng, W., Flocke, F. M., Guenther, A., Keutsch, F. N., Apel, E., and Hansel, A.: Comparison of different real time VOC  
967 measurement techniques in a ponderosa pine forest, *Atmos. Chem. Phys.*, 13, 2893-2906, [https://doi.org/10.5194/acp-13-2893-](https://doi.org/10.5194/acp-13-2893-2013)  
968 2013, 2013.
- 969 Kim, M. J., Novak, G. A., Zuerb, M. C., Yang, M. X., Blomquist, B. W., Huebert, B. J., Cappa, C. D., and Bertram, T. H.: Air-  
970 Sea exchange of biogenic volatile organic compounds and the impact on aerosol particle size distributions, *Geophys Res Lett*, 44,  
971 3887-3896, <https://doi.org/10.1002/2017GL072975>, 2017.
- 972 Kim, P. S., Jacob, D. J., Fisher, J. A., Travis, K., Yu, K., Zhu, L., Yantosca, R. M., Sulprizio, M. P., Jimenez, J. L., Campuzano-  
973 Jost, P., Froyd, K. D., Liao, J., Hair, J. W., Fenn, M. A., Butler, C. F., Wagner, N. L., Gordon, T. D., Welti, A., Wennberg, P. O.,  
974 Crouse, J. D., St Clair, J. M., Teng, A. P., Millet, D. B., Schwarz, J. P., Markovic, M. Z., and Perring, A. E.: Sources,  
975 seasonality, and trends of southeast US aerosol: an integrated analysis of surface, aircraft, and satellite observations with the  
976 GEOS-Chem chemical transport model, *Atmos. Chem. Phys.*, 15, 10411-10433, [https://doi.org/10.5194/acp-15-10411-](https://doi.org/10.5194/acp-15-10411-2015)  
977 2015.
- 978 Kim, S., Huey, L. G., Stickel, R. E., Tanner, D. J., Crawford, J. H., Olson, J. R., Chen, G., Brune, W. H., Ren, X., Leshner, R.,  
979 Wooldridge, P. J., Bertram, T. H., Perring, A., Cohen, R. C., Lefer, B. L., Shetter, R. E., Avery, M., Diskin, G., and Sokolik, I.:  
980 Measurement of HO<sub>2</sub>NO<sub>2</sub> in the free troposphere during the intercontinental chemical transport experiment - North America  
981 2004, *J. Geophys. Res. Atmos.*, 112, <https://doi.org/10.1029/2006jd007676>, 2007.
- 982 Kirkby, J., Duplissy, J., Sengupta, K., Frege, C., Gordon, H., Williamson, C., Heinritzi, M., Simon, M., Yan, C., Almeida, J.,  
983 Trostl, J., Nieminen, T., Ortega, I. K., Wagner, R., Adamov, A., Amorim, A., Bernhammer, A. K., Bianchi, F., Breitenlechner,  
984 M., Brilke, S., Chen, X., Craven, J., Dias, A., Ehrhart, S., Flagan, R. C., Franchin, A., Fuchs, C., Guida, R., Hakala, J., Hoyle, C.  
985 R., Jokinen, T., Junninen, H., Kangasluoma, J., Kim, J., Krapf, M., Kurten, A., Laaksonen, A., Lehtipalo, K., Makhmutov, V.,  
986 Mathot, S., Molteni, U., Onnela, A., Perakyla, O., Piel, F., Petaja, T., Praplan, A. P., Pringle, K., Rap, A., Richards, N. A.,  
987 Riipinen, I., Rissanen, M. P., Rondo, L., Sarnela, N., Schobesberger, S., Scott, C. E., Seinfeld, J. H., Sipila, M., Steiner, G.,  
988 Stozhkov, Y., Stratmann, F., Tome, A., Virtanen, A., Vogel, A. L., Wagner, A. C., Wagner, P. E., Weingartner, E., Wimmer, D.,  
989 Winkler, P. M., Ye, P., Zhang, X., Hansel, A., Dommen, J., Donahue, N. M., Worsnop, D. R., Baltensperger, U., Kulmala, M.,  
990 Carslaw, K. S., and Curtius, J.: Ion-induced nucleation of pure biogenic particles, *Nature*, 533, 521-526,  
991 <https://doi.org/10.1038/nature17953>, 2016.
- 992 Kroll, J. H., Donahue, N. M., Jimenez, J. L., Kessler, S. H., Canagaratna, M. R., Wilson, K. R., Altieri, K. E., Mazzoleni, L. R.,  
993 Wozniak, A. S., Bluhm, H., Mysak, E. R., Smith, J. D., Kolb, C. E., and Worsnop, D. R.: Carbon oxidation state as a metric for  
994 describing the chemistry of atmospheric organic aerosol, *Nat. Chem.*, 3, 133-139, <https://doi.org/10.1038/nchem.948>, 2011.
- 995 Lamarque, J. F., Bond, T. C., Eyring, V., Granier, C., Heil, A., Klimont, Z., Lee, D., Lioussé, C., Mieville, A., Owen, B., Schultz,  
996 M. G., Shindell, D., Smith, S. J., Stehfest, E., Van Aardenne, J., Cooper, O. R., Kainuma, M., Mahowald, N., McConnell, J. R.,  
997 Naik, V., Riahi, K., and van Vuuren, D. P.: Historical (1850-2000) gridded anthropogenic and biomass burning emissions of  
998 reactive gases and aerosols: methodology and application, *Atmos. Chem. Phys.*, 10, 7017-7039, [https://doi.org/10.5194/acp-10-](https://doi.org/10.5194/acp-10-7017-2010)  
999 7017-2010, 2010.
- 1000 Lee, B. H., Lopez-Hilfiker, F. D., Mohr, C., Kurten, T., Worsnop, D. R., and Thornton, J. A.: An iodide-adduct high-resolution  
1001 time-of-flight chemical-ionization mass spectrometer: application to atmospheric inorganic and organic compounds, *Environ.*  
1002 *Sci. Technol.*, 48, 6309-6317, <https://doi.org/10.1021/es500362a>, 2014.
- 1003 Lerner, B. M., Gilman, J. B., Aikin, K. C., Atlas, E. L., Goldan, P. D., Graus, M., Hendershot, R., Isaacman-VanWertz, G. A.,  
1004 Koss, A., Kuster, W. C., Lueb, R. A., McLaughlin, R. J., Peischl, J., Sueper, D., Ryerson, T. B., Tokarek, T. W., Warneke, C.,  
1005 Yuan, B., and de Gouw, J. A.: An improved, automated whole air sampler and gas chromatography mass spectrometry analysis  
1006 system for volatile organic compounds in the atmosphere, *Atmos. Meas. Tech.*, 10, 291-313, [https://doi.org/10.5194/amt-10-291-](https://doi.org/10.5194/amt-10-291-2017)  
1007 2017, 2017.

- 1008 Li, J., Mao, J., Min, K. E., Washenfelder, R. A., Brown, S. S., Kaiser, J., Keutsch, F. N., Volkamer, R., Wolfe, G. M., Hanisco, T.  
1009 F., Pollack, I. B., Ryerson, T. B., Graus, M., Gilman, J. B., Lerner, B. M., Warneke, C., de Gouw, J. A., Middlebrook, A. M.,  
1010 Liao, J., Welti, A., Henderson, B. H., McNeill, V. F., Hall, S. R., Ullmann, K., Donner, L. J., Paulot, F., and Horowitz, L. W.:  
1011 Observational constraints on glyoxal production from isoprene oxidation and its contribution to organic aerosol over the  
1012 Southeast United States, *J. Geophys. Res. Atmos.*, 121, 9849-9861, <https://doi.org/10.1002/2016JD025331>, 2016.
- 1013 Li, S. M., Leithead, A., Moussa, S. G., Liggio, J., Moran, M. D., Wang, D., Hayden, K., Darlington, A., Gordon, M., Staebler, R.,  
1014 Makar, P. A., Stroud, C. A., McLaren, R., Liu, P. S. K., O'Brien, J., Mittermeier, R. L., Zhang, J., Marson, G., Cober, S. G.,  
1015 Wolde, M., and Wentzell, J. J. B.: Differences between measured and reported volatile organic compound emissions from oil  
1016 sands facilities in Alberta, Canada, *Proc. Natl. Acad. Sci. U.S.A.*, 114, E3756-E3765, <https://doi.org/10.1073/pnas.1617862114>,  
1017 2017.
- 1018 Lin, J. T., and McElroy, M. B.: Impacts of boundary layer mixing on pollutant vertical profiles in the lower troposphere:  
1019 Implications to satellite remote sensing, *Atmos. Environ.*, 44, 1726-1739, <https://doi.org/10.1016/j.atmosenv.2010.02.009>, 2010.
- 1020 Lin, S. J., and Rood, R. B.: Multidimensional flux-form semi-Lagrangian transport schemes, *Mon Weather Rev*, 124, 2046-2070,  
1021 [https://doi.org/10.1175/1520-0493\(1996\)124<2046:Mffslt>2.0.Co;2](https://doi.org/10.1175/1520-0493(1996)124<2046:Mffslt>2.0.Co;2), 1996.
- 1022 Long, M. S., Yantosca, R., Nielsen, J. E., Keller, C. A., da Silva, A., Sulprizio, M. P., Pawson, S., and Jacob, D. J.: Development  
1023 of a grid-independent GEOS-Chem chemical transport model (v9-02) as an atmospheric chemistry module for Earth system  
1024 models, *Geosci Model Dev*, 8, 595-602, <https://doi.org/10.5194/gmd-8-595-2015>, 2015.
- 1025 Luo, G., and Yu, F.: A numerical evaluation of global oceanic emissions of alpha-pinene and isoprene, *Atmos. Chem. Phys.*, 10,  
1026 2007-2015, <https://doi.org/10.5194/acp-10-2007-2010>, 2010.
- 1027 Mao, J., Ren, X., Brune, W. H., Olson, J. R., Crawford, J. H., Fried, A., Huey, L. G., Cohen, R. C., Heikes, B., Singh, H. B.,  
1028 Blake, D. R., Sachse, G. W., Diskin, G. S., Hall, S. R., and Shetter, R. E.: Airborne measurement of OH reactivity during  
1029 INTEX-B, *Atmos. Chem. Phys.*, 9, 163-173, <https://doi.org/10.5194/acp-9-163-2009>, 2009.
- 1030 Marais, E. A., Jacob, D. J., Jimenez, J. L., Campuzano-Jost, P., Day, D. A., Hu, W., Krechmer, J., Zhu, L., Kim, P. S., Miller, C.  
1031 C., Fisher, J. A., Travis, K., Yu, K., Hanisco, T. F., Wolfe, G. M., Arkinson, H. L., Pye, H. O. T., Froyd, K. D., Liao, J., and  
1032 McNeill, V. F.: Aqueous-phase mechanism for secondary organic aerosol formation from isoprene: application to the southeast  
1033 United States and co-benefit of SO<sub>2</sub> emission controls, *Atmos. Chem. Phys.*, 16, 1603-1618, <https://doi.org/10.5194/acp-16-1603-2016>, 2016.
- 1035 Marandino, C. A., De Bruyn, W. J., Miller, S. D., Prather, M. J., and Saltzman, E. S.: Oceanic uptake and the global atmospheric  
1036 acetone budget, *Geophys Res Lett*, 32, <https://doi.org/10.1029/2005gl023285>, 2005.
- 1037 Mari, C., Jacob, D. J., and Bechtold, P.: Transport and scavenging of soluble gases in a deep convective cloud, *J. Geophys. Res.*  
1038 *Atmos.*, 105, 22255-22267, <https://doi.org/10.1029/2000jd900211>, 2000.
- 1039 McDonald, B. C., Gentner, D. R., Goldstein, A. H., and Harley, R. A.: Long-term trends in motor vehicle emissions in u.s. urban  
1040 areas, *Environ. Sci. Technol.*, 47, 10022-10031, <https://doi.org/10.1021/es401034z>, 2013.
- 1041 McDonald, B. C., de Gouw, J. A., Gilman, J. B., Jathar, S. H., Akherati, A., Cappa, C. D., Jimenez, J. L., Lee-Taylor, J., Hayes,  
1042 P. L., McKeen, S. A., Cui, Y. Y., Kim, S. W., Gentner, D. R., Isaacman-VanWertz, G., Goldstein, A. H., Harley, R. A., Frost, G.  
1043 J., Roberts, J. M., Ryerson, T. B., and Trainer, M.: Volatile chemical products emerging as largest petrochemical source of urban  
1044 organic emissions, *Science*, 359, 760-764, <https://doi.org/10.1126/science.aaq0524>, 2018.
- 1045 Miller, C. C., Jacob, D. J., Marais, E. A., Yu, K. R., Travis, K. R., Kim, P. S., Fisher, J. A., Zhu, L., Wolfe, G. M., Hanisco, T. F.,  
1046 Keutsch, F. N., Kaiser, J., Min, K. E., Brown, S. S., Washenfelder, R. A., Abad, G. G., and Chance, K.: Glyoxal yield from  
1047 isoprene oxidation and relation to formaldehyde: chemical mechanism, constraints from SENEX aircraft observations, and  
1048 interpretation of OMI satellite data, *Atmos. Chem. Phys.*, 17, 8725-8738, <https://doi.org/10.5194/acp-17-8725-2017>, 2017.
- 1049 Millet, D. B., Jacob, D. J., Custer, T. G., de Gouw, J. A., Goldstein, A. H., Karl, T., Singh, H. B., Sive, B. C., Talbot, R. W.,  
1050 Warneke, C., and Williams, J.: New constraints on terrestrial and oceanic sources of atmospheric methanol, *Atmos. Chem. Phys.*,  
1051 8, 6887-6905, <https://doi.org/10.5194/acp-8-6887-2008>, 2008.
- 1052 Millet, D. B., Guenther, A., Siegel, D. A., Nelson, N. B., Singh, H. B., de Gouw, J. A., Warneke, C., Williams, J., Eerdekens, G.,  
1053 Sinha, V., Karl, T., Flocke, F., Apel, E., Riemer, D. D., Palmer, P. I., and Barkley, M.: Global atmospheric budget of

- 1054 acetaldehyde: 3-D model analysis and constraints from in-situ and satellite observations, *Atmos. Chem. Phys.*, 10, 3405-3425,  
1055 <https://doi.org/10.5194/acp-10-3405-2010>, 2010.
- 1056 Millet, D. B., Apel, E., Henze, D. K., Hill, J., Marshall, J. D., Singh, H. B., and Tessum, C. W.: Natural and anthropogenic  
1057 ethanol sources in North America and potential atmospheric impacts of ethanol fuel use, *Environ. Sci. Technol.*, 46, 8484-8492,  
1058 <https://doi.org/10.1021/es300162u>, 2012.
- 1059 Millet, D. B., Baasandorj, M., Farmer, D. K., Thornton, J. A., Baumann, K., Brophy, P., Chaliyakunnel, S., de Gouw, J. A.,  
1060 Graus, M., Hu, L., Koss, A., Lee, B. H., Lopez-Hilfiker, F. D., Neuman, J. A., Paulot, F., Peischl, J., Pollack, I. B., Ryerson, T.  
1061 B., Warneke, C., Williams, B. J., and Xu, J.: A large and ubiquitous source of atmospheric formic acid, *Atmos. Chem. Phys.*, 15,  
1062 6283-6304, <https://doi.org/10.5194/acp-15-6283-2015>, 2015.
- 1063 Millet, D. B., Alwe, H. D., Chen, X., Deventer, M. J., Griffis, T. J., Holzinger, R., Bertman, S. B., Rickly, P. S., Stevens, P. S.,  
1064 Leonardis, T., Locoge, N., Dusanter, S., Tyndall, G. S., Alvarez, S. L., Erickson, M. H., and Flynn, J. H.: Bidirectional  
1065 ecosystem-atmosphere fluxes of volatile organic compounds across the mass spectrum: How many matter?, *Acs Earth Space*  
1066 *Chem*, 2, 764-777, <https://doi.org/10.1021/acsearthspacechem.8b00061>, 2018.
- 1067 Min, K. E., Washenfelder, R. A., Dube, W. P., Langford, A. O., Edwards, P. M., Zarzana, K. J., Stutz, J., Lu, K., Rohrer, F.,  
1068 Zhang, Y., and Brown, S. S.: A broadband cavity enhanced absorption spectrometer for aircraft measurements of glyoxal,  
1069 methylglyoxal, nitrous acid, nitrogen dioxide, and water vapor, *Atmos. Meas. Tech.*, 9, 423-440, <https://doi.org/10.5194/amt-9-423-2016>, 2016.
- 1071 Müller, J. F., Liu, Z., Nguyen, V. S., Stavrou, T., Harvey, J. N., and Peeters, J.: The reaction of methyl peroxy and hydroxyl  
1072 radicals as a major source of atmospheric methanol, *Nat. Commun.*, 7, 13213, <https://doi.org/10.1038/ncomms13213>, 2016a.
- 1073 Müller, M., Mikoviny, T., Feil, S., Haidacher, S., Hanel, G., Hartungen, E., Jordan, A., Mark, L., Mutschlechner, P.,  
1074 Schottkowsky, R., Sulzer, P., Crawford, J. H., and Wisthaler, A.: A compact PTR-ToF-MS instrument for airborne measurements  
1075 of volatile organic compounds at high spatiotemporal resolution, *Atmos. Meas. Tech.*, 7, 3763-3772, <https://doi.org/10.5194/amt-7-3763-2014>, 2014.
- 1077 Müller, M., Anderson, B. E., Beyersdorf, A. J., Crawford, J. H., Diskin, G. S., Eichler, P., Fried, A., Keutsch, F. N., Mikoviny,  
1078 T., Thornhill, K. L., Walega, J. G., Weinheimer, A. J., Yang, M., Yokelson, R. J., and Wisthaler, A.: In situ measurements and  
1079 modeling of reactive trace gases in a small biomass burning plume, *Atmos. Chem. Phys.*, 16, 3813-3824,  
1080 <https://doi.org/10.5194/acp-16-3813-2016>, 2016b.
- 1081 Mungall, E. L., Abbatt, J. P. D., Wentzell, J. J. B., Lee, A. K. Y., Thomas, J. L., Blais, M., Gosselin, M., Miller, L. A.,  
1082 Papakyriakou, T., Willis, M. D., and Liggio, J.: Microlayer source of oxygenated volatile organic compounds in the summertime  
1083 marine Arctic boundary layer, *Proc. Natl. Acad. Sci. U.S.A.*, 114, 6203-6208, <https://doi.org/10.1073/pnas.1620571114>, 2017.
- 1084 Myhre, G., Shindell, D., Bréon, F.-M., Collins, W., Fuglestedt, J., Huang, J., Koch, D., Lamarque, J.-F., Lee, D., Mendoza, B.,  
1085 Nakajima, T., Robock, A., Stephens, G., Takemura, T., and Zhang, H.: Anthropogenic and natural radiative forcing, in: *Climate*  
1086 *Change 2013: The Physical Science Basis. Contribution of Working Group I to the Fifth Assessment Report of the*  
1087 *Intergovernmental Panel on Climate Change*, edited by: Stocker, T. F., Qin, D., Plattner, G.-K., Tignor, M., Allen, S. K.,  
1088 Boschung, J., Nauels, A., Xia, Y., Bex, V., and Midgley, P. M., Cambridge University Press, Cambridge, United Kingdom and  
1089 New York, NY, USA, 659-740, 2013.
- 1090 Nguyen, T. B., Crounse, J. D., Teng, A. P., St Clair, J. M., Paulot, F., Wolfe, G. M., and Wennberg, P. O.: Rapid deposition of  
1091 oxidized biogenic compounds to a temperate forest, *Proc. Natl. Acad. Sci. U.S.A.*, 112, E392-401,  
1092 <https://doi.org/10.1073/pnas.1418702112>, 2015.
- 1093 Nirmalakhandan, N. N., and Speece, R. E.: QSAR model for predicting Henry's constant, *Environ. Sci. Technol.*, 22, 1349-1357,  
1094 <https://doi.org/10.1021/es00176a016>, 1988.
- 1095 O'Sullivan, D. W., Silwal, I. K. C., McNeill, A. S., Treadaway, V., and Heikes, B. G.: Quantification of gas phase hydrogen  
1096 peroxide and methyl peroxide in ambient air: Using atmospheric pressure chemical ionization mass spectrometry with O<sub>2</sub><sup>-</sup>, and  
1097 O<sub>2</sub>-(CO<sub>2</sub>) reagent ions, *Int. J. Mass Spectrom.*, 424, 16-26, <https://doi.org/10.1016/j.ijms.2017.11.015>, 2018.
- 1098 Osthoff, H. D., Roberts, J. M., Ravishankara, A. R., Williams, E. J., Lerner, B. M., Sommariva, R., Bates, T. S., Coffman, D.,  
1099 Quinn, P. K., Dibb, J. E., Stark, H., Burkholder, J. B., Talukdar, R. K., Meagher, J., Fehsenfeld, F. C., and Brown, S. S.: High

- 1100 levels of nitril chloride in the polluted subtropical marine boundary layer, *Nat Geosci*, 1, 324-328,  
1101 <https://doi.org/10.1038/ngeo177>, 2008.
- 1102 Palmer, P. I., and Shaw, S. L.: Quantifying global marine isoprene fluxes using MODIS chlorophyll observations, *Geophys Res*  
1103 *Lett*, 32, <https://doi.org/10.1029/2005gl022592>, 2005.
- 1104 Park, J. H., Goldstein, A. H., Timkovsky, J., Fares, S., Weber, R., Karlik, J., and Holzinger, R.: Active atmosphere-ecosystem  
1105 exchange of the vast majority of detected volatile organic compounds, *Science*, 341, 643-647,  
1106 <https://doi.org/10.1126/science.1235053>, 2013.
- 1107 Parrish, D. D.: Critical evaluation of US on-road vehicle emission inventories, *Atmos. Environ.*, 40, 2288-2300,  
1108 <https://doi.org/10.1016/j.atmosenv.2005.11.033>, 2006.
- 1109 Paulot, F., Crounse, J. D., Kjaergaard, H. G., Kroll, J. H., Seinfeld, J. H., and Wennberg, P. O.: Isoprene photooxidation: new  
1110 insights into the production of acids and organic nitrates, *Atmos. Chem. Phys.*, 9, 1479-1501, [https://doi.org/10.5194/acp-9-1479-](https://doi.org/10.5194/acp-9-1479-2009)  
1111 2009, 2009a.
- 1112 Paulot, F., Crounse, J. D., Kjaergaard, H. G., Kurten, A., St Clair, J. M., Seinfeld, J. H., and Wennberg, P. O.: Unexpected  
1113 epoxide formation in the gas-phase photooxidation of isoprene, *Science*, 325, 730-733, [10.1126/science.1172910](https://doi.org/10.1126/science.1172910), 2009b.
- 1114 Paulot, F., Wunch, D., Crounse, J. D., Toon, G. C., Millet, D. B., DeCarlo, P. F., Vigouroux, C., Deutscher, N. M., Abad, G. G.,  
1115 Notholt, J., Warneke, T., Hannigan, J. W., Warneke, C., de Gouw, J. A., Dunlea, E. J., De Maziere, M., Griffith, D. W. T.,  
1116 Bernath, P., Jimenez, J. L., and Wennberg, P. O.: Importance of secondary sources in the atmospheric budgets of formic and  
1117 acetic acids, *Atmos. Chem. Phys.*, 11, 1989-2013, <https://doi.org/10.5194/acp-11-1989-2011>, 2011.
- 1118 Peischl, J., Ryerson, T. B., Holloway, J. S., Trainer, M., Andrews, A. E., Atlas, E. L., Blake, D. R., Daube, B. C., Dlugokencky,  
1119 E. J., Fischer, M. L., Goldstein, A. H., Guha, A., Karl, T., Kofler, J., Kosciuch, E., Misztal, P. K., Perring, A. E., Pollack, I. B.,  
1120 Santoni, G. W., Schwarz, J. P., Spackman, J. R., Wofsy, S. C., and Parrish, D. D.: Airborne observations of methane emissions  
1121 from rice cultivation in the Sacramento Valley of California, *J. Geophys. Res. Atmos.*, 117, n/a-n/a,  
1122 <https://doi.org/10.1029/2012jd017994>, 2012.
- 1123 Pfister, G., Flocke, F., Hornbrook, R., Orlando, J., Lee, S., and Schroeder, J.: FRAPPÉ Final Report: Process-Based and Regional  
1124 Source Impact Analysis for FRAPPÉ and DISCOVER-AQ 2014, available at:  
1125 [https://www.colorado.gov/airquality/tech\\_doc\\_repository.aspx?action=open&file=FRAPPE-NCAR\\_Final\\_Report\\_July2017.pdf](https://www.colorado.gov/airquality/tech_doc_repository.aspx?action=open&file=FRAPPE-NCAR_Final_Report_July2017.pdf),  
1126 last access: 13 Jan 2019, 2017.
- 1127 Philip, S., Martin, R. V., and Keller, C. A.: Sensitivity of chemistry-transport model simulations to the duration of chemical and  
1128 transport operators: a case study with GEOS-Chem v10-01, *Geosci Model Dev*, 9, 1683-1695, [https://doi.org/10.5194/gmd-9-](https://doi.org/10.5194/gmd-9-1683-2016)  
1129 1683-2016, 2016.
- 1130 Pollack, I. B., Lerner, B. M., and Ryerson, T. B.: Evaluation of ultraviolet light-emitting diodes for detection of atmospheric NO<sub>2</sub>  
1131 by photolysis - chemiluminescence, *J. Atmos. Chem.*, 65, 111-125, <https://doi.org/10.1007/s10874-011-9184-3>, 2010.
- 1132 Praske, E., Otkjaer, R. V., Crounse, J. D., Hethcox, J. C., Stoltz, B. M., Kjaergaard, H. G., and Wennberg, P. O.: Atmospheric  
1133 autoxidation is increasingly important in urban and suburban North America, *Proc. Natl. Acad. Sci. U.S.A.*, 115, 64-69,  
1134 <https://doi.org/10.1073/pnas.1715540115>, 2018.
- 1135 Read, K. A., Mahajan, A. S., Carpenter, L. J., Evans, M. J., Faria, B. V., Heard, D. E., Hopkins, J. R., Lee, J. D., Moller, S. J.,  
1136 Lewis, A. C., Mendes, L., McQuaid, J. B., Oetjen, H., Saiz-Lopez, A., Pilling, M. J., and Plane, J. M.: Extensive halogen-  
1137 mediated ozone destruction over the tropical Atlantic Ocean, *Nature*, 453, 1232-1235, <https://doi.org/10.1038/nature07035>, 2008.
- 1138 Read, K. A., Carpenter, L. J., Arnold, S. R., Beale, R., Nightingale, P. D., Hopkins, J. R., Lewis, A. C., Lee, J. D., Mendes, L.,  
1139 and Pickering, S. J.: Multiannual observations of acetone, methanol, and acetaldehyde in remote tropical atlantic air: implications  
1140 for atmospheric OVOC budgets and oxidative capacity, *Environ. Sci. Technol.*, 46, 11028-11039,  
1141 <https://doi.org/10.1021/es302082p>, 2012.
- 1142 Riahi, K., Grubler, A., and Nakicenovic, N.: Scenarios of long-term socio-economic and environmental development under  
1143 climate stabilization, *Technol. Forecasting Social Change*, 74, 887-935, <https://doi.org/10.1016/j.techfore.2006.05.026>, 2007.

- 1144 Richter, D., Weibring, P., Walega, J. G., Fried, A., Spuler, S. M., and Taubman, M. S.: Compact highly sensitive multi-species  
1145 airborne mid-IR spectrometer, *Appl. Phys. B: Lasers Opt.*, 119, 119-131, <https://doi.org/10.1007/s00340-015-6038-8>, 2015.
- 1146 Ryerson, T. B., Buhr, M. P., Frost, G. J., Goldan, P. D., Holloway, J. S., Hubler, G., Jobson, B. T., Kuster, W. C., McKeen, S. A.,  
1147 Parrish, D. D., Roberts, J. M., Sueper, D. T., Trainer, M., Williams, J., and Fehsenfeld, F. C.: Emissions lifetimes and ozone  
1148 formation in power plant plumes, *J. Geophys. Res. Atmos.*, 103, 22569-22583, <https://doi.org/10.1029/98jd01620>, 1998.
- 1149 Ryerson, T. B., Huey, L. G., Knapp, K., Neuman, J. A., Parrish, D. D., Sueper, D. T., and Fehsenfeld, F. C.: Design and initial  
1150 characterization of an inlet for gas-phase NO<sub>y</sub> measurements from aircraft, *J. Geophys. Res. Atmos.*, 104, 5483-5492,  
1151 <https://doi.org/10.1029/1998jd100087>, 1999.
- 1152 Ryerson, T. B., Andrews, A. E., Angevine, W. M., Bates, T. S., Brock, C. A., Cairns, B., Cohen, R. C., Cooper, O. R., de Gouw,  
1153 J. A., Fehsenfeld, F. C., Ferrare, R. A., Fischer, M. L., Flagan, R. C., Goldstein, A. H., Hair, J. W., Hardesty, R. M., Hostetler, C.  
1154 A., Jimenez, J. L., Langford, A. O., McCauley, E., McKeen, S. A., Molina, L. T., Nenes, A., Oltmans, S. J., Parrish, D. D.,  
1155 Pederson, J. R., Pierce, R. B., Prather, K., Quinn, P. K., Seinfeld, J. H., Senff, C. J., Sorooshian, A., Stutz, J., Surratt, J. D.,  
1156 Trainer, M., Volkamer, R., Williams, E. J., and Wofsy, S. C.: The 2010 California Research at the Nexus of Air Quality and  
1157 Climate Change (CalNex) field study, *J. Geophys. Res. Atmos.*, 118, 5830-5866, <https://doi.org/10.1002/jgrd.50331>, 2013.
- 1158 Safieddine, S. A., Heald, C. L., and Henderson, B. H.: The global nonmethane reactive organic carbon budget: A modeling  
1159 perspective, *Geophys Res Lett*, 44, 3897-3906, <https://doi.org/10.1002/2017GL072602>, 2017.
- 1160 Sander, R.: Compilation of Henry's law constants (version 4.0) for water as solvent, *Atmos. Chem. Phys.*, 15, 4399-4981,  
1161 <https://doi.org/10.5194/acp-15-4399-2015>, 2015.
- 1162 Schauffler, S. M., Atlas, E. L., Donnelly, S. G., Andrews, A., Montzka, S. A., Elkins, J. W., Hurst, D. F., Romashkin, P. A.,  
1163 Dutton, G. S., and Stroud, V.: Chlorine budget and partitioning during the Stratospheric Aerosol and Gas Experiment (SAGE) III  
1164 Ozone Loss and Validation Experiment (SOLVE), *J. Geophys. Res. Atmos.*, 108, <https://doi.org/10.1029/2001jd002040>, 2003.
- 1165 SEAC<sup>4</sup>RS Science Team: SEAC<sup>4</sup>RS Field Campaign Data. NASA Langley Atmospheric Science Data Center DAAC,  
1166 <https://doi.org/10.5067/aircraft/seac4rs/aerosol-tracegas-cloud>, 2013.
- 1167 Shaw, M. F., Sztáray, B., Whalley, L. K., Heard, D. E., Millet, D. B., Jordan, M. J., Osborn, D. L., and Kable, S. H.: Photo-  
1168 tautomerization of acetaldehyde as a photochemical source of formic acid in the troposphere, *Nat. Commun.*, 9, 2584, 2018.
- 1169 Shaw, S. L., Gantt, B., and Meskhidze, N.: Production and emissions of marine isoprene and monoterpenes: A review, *Adv  
1170 Meteorol*, 2010, 1-24, <https://doi.org/10.1155/2010/408696>, 2010.
- 1171 Singh, H. B., Tabazadeh, A., Evans, M. J., Field, B. D., Jacob, D. J., Sachse, G., Crawford, J. H., Shetter, R., and Brune, W. H.:  
1172 Oxygenated volatile organic chemicals in the oceans: Inferences and implications based on atmospheric observations and air-sea  
1173 exchange models, *Geophys Res Lett*, 30, <https://doi.org/10.1029/2003gl017933>, 2003.
- 1174 Slusher, D. L., Huey, L. G., Tanner, D. J., Flocke, F. M., and Roberts, J. M.: A thermal dissociation-chemical ionization mass  
1175 spectrometry (TD-CIMS) technique for the simultaneous measurement of peroxyacyl nitrates and dinitrogen pentoxide, *J.  
1176 Geophys. Res. Atmos.*, 109, <https://doi.org/10.1029/2004jd004670>, 2004.
- 1177 St Clair, J. M., McCabe, D. C., Crouse, J. D., Steiner, U., and Wennberg, P. O.: Chemical ionization tandem mass spectrometer  
1178 for the in situ measurement of methyl hydrogen peroxide, *Rev. Sci. Instrum.*, 81, 094102, <https://doi.org/10.1063/1.3480552>,  
1179 2010.
- 1180 Staudinger, J., and Roberts, P. V.: A critical compilation of Henry's law constant temperature dependence relations for organic  
1181 compounds in dilute aqueous solutions, *Chemosphere*, 44, 561-576, [https://doi.org/10.1016/S0045-6535\(00\)00505-1](https://doi.org/10.1016/S0045-6535(00)00505-1), 2001.
- 1182 Stavrou, T., Muller, J. F., Peeters, J., Razavi, A., Clarisse, L., Clerbaux, C., Coheur, P. F., Hurtmans, D., De Maziere, M.,  
1183 Vigouroux, C., Deutscher, N. M., Griffith, D. W. T., Jones, N., and Paton-Walsh, C.: Satellite evidence for a large source of  
1184 formic acid from boreal and tropical forests, *Nat Geosci*, 5, 26-30, <https://doi.org/10.1038/NGEO1354>, 2012.
- 1185 Stettler, M. E. J., Eastham, S., and Barrett, S. R. H.: Air quality and public health impacts of UK airports. Part I: Emissions,  
1186 *Atmos. Environ.*, 45, 5415-5424, <https://doi.org/10.1016/j.atmosenv.2011.07.012>, 2011.

- 1187 Toon, O. B., Maring, H., Dibb, J., Ferrare, R., Jacob, D. J., Jensen, E. J., Luo, Z. J., Mace, G. G., Pan, L. L., Pfister, L., Rosenlof,  
1188 K. H., Redemann, J., Reid, J. S., Singh, H. B., Thompson, A. M., Yokelson, R., Minnis, P., Chen, G., Jucks, K. W., and Pszenny,  
1189 A.: Planning, implementation, and scientific goals of the Studies of Emissions and Atmospheric Composition, Clouds and  
1190 Climate Coupling by Regional Surveys (SEAC(4)RS) field mission, *J. Geophys. Res. Atmos.*, 121, 4967-5009,  
1191 <https://doi.org/10.1002/2015JD024297>, 2016.
- 1192 Travis, K. R., Jacob, D. J., Fisher, J. A., Kim, P. S., Marais, E. A., Zhu, L., Yu, K., Miller, C. C., Yantosca, R. M., Sulprizio, M.  
1193 P., Thompson, A. M., Wennberg, P. O., Crounse, J. D., St Clair, J. M., Cohen, R. C., Laughner, J. L., Dibb, J. E., Hall, S. R.,  
1194 Ullmann, K., Wolfe, G. M., Pollack, I. B., Peischl, J., Neuman, J. A., and Zhou, X.: Why do Models Overestimate Surface Ozone  
1195 in the Southeastern United States?, *Atmos. Chem. Phys.*, 16, 13561-13577, <https://doi.org/10.5194/acp-16-13561-2016>, 2016.
- 1196 Treadaway, V., Heikes, B. G., McNeill, A. S., Silwal, I. K. C., and O'Sullivan, D. W.: Measurement of formic acid, acetic acid  
1197 and hydroxyacetaldehyde, hydrogen peroxide, and methyl peroxide in air by chemical ionization mass spectrometry: airborne  
1198 method development, *Atmos. Meas. Tech.*, 11, 1901-1920, <https://doi.org/10.5194/amt-11-1901-2018>, 2018.
- 1199 Trostl, J., Chuang, W. K., Gordon, H., Heinritzi, M., Yan, C., Molteni, U., Ahlm, L., Frege, C., Bianchi, F., Wagner, R., Simon,  
1200 M., Lehtipalo, K., Williamson, C., Craven, J. S., Duplissy, J., Adamov, A., Almeida, J., Bernhammer, A. K., Breitenlechner, M.,  
1201 Brilke, S., Dias, A., Ehrhart, S., Flagan, R. C., Franchin, A., Fuchs, C., Guida, R., Gysel, M., Hansel, A., Hoyle, C. R., Jokinen,  
1202 T., Junninen, H., Kangasluoma, J., Keskinen, H., Kim, J., Krapf, M., Kurten, A., Laaksonen, A., Lawler, M., Leiminger, M.,  
1203 Mathot, S., Mohler, O., Nieminen, T., Onnela, A., Petaja, T., Piel, F. M., Miettinen, P., Rissanen, M. P., Rondo, L., Sarnela, N.,  
1204 Schobesberger, S., Sengupta, K., Sipila, M., Smith, J. N., Steiner, G., Tome, A., Virtanen, A., Wagner, A. C., Weingartner, E.,  
1205 Wimmer, D., Winkler, P. M., Ye, P. L., Carslaw, K. S., Curtius, J., Dommen, J., Kirkby, J., Kulmala, M., Riipinen, I., Worsnop,  
1206 D. R., Donahue, N. M., and Baltensperger, U.: The role of low-volatility organic compounds in initial particle growth in the  
1207 atmosphere, *Nature*, 533, 527-+, <https://doi.org/10.1038/nature18271>, 2016.
- 1208 van der Werf, G. R., Randerson, J. T., Giglio, L., van Leeuwen, T. T., Chen, Y., Rogers, B. M., Mu, M. Q., van Marle, M. J. E.,  
1209 Morton, D. C., Collatz, G. J., Yokelson, R. J., and Kasibhatla, P. S.: Global fire emissions estimates during 1997-2016, *Earth  
1210 Syst. Sci. Data*, 9, 697-720, <https://doi.org/10.5194/essd-9-697-2017>, 2017.
- 1211 van Vuuren, D. P., Edmonds, J., Kainuma, M., Riahi, K., Thomson, A., Hibbard, K., Hurtt, G. C., Kram, T., Krey, V., Lamarque,  
1212 J. F., Masui, T., Meinshausen, M., Nakicenovic, N., Smith, S. J., and Rose, S. K.: The representative concentration pathways: an  
1213 overview, *Clim. Change*, 109, 5-31, <https://doi.org/10.1007/s10584-011-0148-z>, 2011.
- 1214 Wang, Y. H., Jacob, D. J., and Logan, J. A.: Global simulation of tropospheric O<sub>3</sub>-NO<sub>x</sub>-hydrocarbon chemistry 1. Model  
1215 formulation, *J. Geophys. Res. Atmos.*, 103, 10713-10725, <https://doi.org/10.1029/98jd00158>, 1998.
- 1216 Warneke, C., de Gouw, J. A., Nowak, J. B., and Peischl, J.: Volatile organic compound emissions from agriculture in Central  
1217 Valley, California, *Abstr. Pap. Am. Chem. Soc.*, 242, 1, 2011.
- 1218 Warneke, C., de Gouw, J. A., Holloway, J. S., Peischl, J., Ryerson, T. B., Atlas, E., Blake, D., Trainer, M., and Parrish, D. D.:  
1219 Multiyear trends in volatile organic compounds in Los Angeles, California: Five decades of decreasing emissions, *J. Geophys.  
1220 Res. Atmos.*, 117, n/a-n/a, <https://doi.org/10.1029/2012jd017899>, 2012.
- 1221 Warneke, C., Geiger, F., Edwards, P. M., Dube, W., Petron, G., Kofler, J., Zahn, A., Brown, S. S., Graus, M., Gilman, J. B.,  
1222 Lerner, B. M., Peischl, J., Ryerson, T. B., de Gouw, J. A., and Roberts, J. M.: Volatile organic compound emissions from the oil  
1223 and natural gas industry in the Uintah Basin, Utah: oil and gas well pad emissions compared to ambient air composition, *Atmos.  
1224 Chem. Phys.*, 14, 10977-10988, <https://doi.org/10.5194/acp-14-10977-2014>, 2014.
- 1225 Warneke, C., Trainer, M., de Gouw, J. A., Parrish, D. D., Fahey, D. W., Ravishankara, A. R., Middlebrook, A. M., Brock, C. A.,  
1226 Roberts, J. M., Brown, S. S., Neuman, J. A., Lerner, B. M., Lack, D., Law, D., Hubler, G., Pollack, I., Sjostedt, S., Ryerson, T.  
1227 B., Gilman, J. B., Liao, J., Holloway, J., Peischl, J., Nowak, J. B., Aikin, K., Min, K. E., Washenfelder, R. A., Graus, M. G.,  
1228 Richardson, M., Markovic, M. Z., Wagner, N. L., Welti, A., Veres, P. R., Edwards, P., Schwarz, J. P., Gordon, T., Dube, W. P.,  
1229 McKeen, S., Brioude, J., Ahmadov, R., Bougiatioti, A., Lin, J. J., Nenes, A., Wolfe, G. M., Hanisco, T. F., Lee, B. H., Lopez-  
1230 Hilfiker, F. D., Thornton, J. A., Keutsch, F. N., Kaiser, J., Mao, J., and Hatch, C.: Instrumentation and measurement strategy for  
1231 the NOAA SENEX aircraft campaign as part of the Southeast Atmosphere Study 2013, *Atmos. Meas. Tech.*, 9, 3063-3093,  
1232 <https://doi.org/10.5194/amt-9-3063-2016>, 2016.
- 1233 Weibring, P., Richter, D., Walega, J. G., Rippe, L., and Fried, A.: Difference frequency generation spectrometer for simultaneous  
1234 multispecies detection, *Opt. Express*, 18, 27670-27681, <https://doi.org/10.1364/OE.18.027670>, 2010.



- 1235 Weinheimer, A. J., Walega, J. G., Ridley, B. A., Gary, B. L., Blake, D. R., Blake, N. J., Rowland, F. S., Sachse, G. W.,  
 1236 Anderson, B. E., and Collins, J. E.: Meridional distributions of NO<sub>x</sub>, NO<sub>y</sub> and other species in the lower stratosphere and upper  
 1237 troposphere during AASE II, *Geophys Res Lett*, 21, 2583-2586, <https://doi.org/10.1029/94gl01897>, 1994.
- 1238 Wells, K. C., Millet, D. B., Hu, L., Cady-Pereira, K. E., Xiao, Y., Shephard, M. W., Clerbaux, C. L., Clarisse, L., Coheur, P. F.,  
 1239 Apel, E. C., de Gouw, J., Warneke, C., Singh, H. B., Goldstein, A. H., and Sive, B. C.: Tropospheric methanol observations from  
 1240 space: retrieval evaluation and constraints on the seasonality of biogenic emissions, *Atmos. Chem. Phys.*, 12, 5897-5912,  
 1241 <https://doi.org/10.5194/acp-12-5897-2012>, 2012.
- 1242 Wesely, M. L.: Parameterization of surface resistances to gaseous dry deposition in regional-scale numerical models, *Atmos.*  
 1243 *Environ.*, 23, 1293-1304, [https://doi.org/10.1016/0004-6981\(89\)90153-4](https://doi.org/10.1016/0004-6981(89)90153-4), 1989.
- 1244 Wiedinmyer, C., Akagi, S. K., Yokelson, R. J., Emmons, L. K., Al-Saadi, J. A., Orlando, J. J., and Soja, A. J.: The Fire  
 1245 INventory from NCAR (FINN): a high resolution global model to estimate the emissions from open burning, *Geosci Model Dev*,  
 1246 4, 625-641, <https://doi.org/10.5194/gmd-4-625-2011>, 2011.
- 1247 Williams, J., Holzinger, R., Gros, V., Xu, X., Atlas, E., and Wallace, D. W. R.: Measurements of organic species in air and  
 1248 seawater from the tropical Atlantic, *Geophys Res Lett*, 31, <https://doi.org/10.1029/2004gl020012>, 2004.
- 1249 Wisthaler, A., Hansel, A., Dickerson, R. R., and Crutzen, P. J.: Organic trace gas measurements by PTR-MS during INDOEX  
 1250 1999, *J. Geophys. Res. Atmos.*, 107, <https://doi.org/10.1029/2001jd000576>, 2002.
- 1251 Wofsy, S. C., Afshar, S., Allen, H. M., Apel, E., Asher, E. C., Barletta, B., Bent, J., Bian, H., Biggs, B. C., Blake, D. R., Blake,  
 1252 N., Bourgeois, I., Brock, C. A., Brune, W. H., Budney, J. W., Bui, T. P., Butler, A., Campuzano-Jost, P., Chang, C. S., Chin, M.,  
 1253 Commane, R., Correa, G., Crounse, J. D., Cullis, P. D., Daube, B. C., Day, D. A., Dean-Day, J. M., Dibb, J. E., DiGangi, J. P.,  
 1254 Diskin, G. S., Dollner, M., Elkins, J. W., Erdesz, F., Fiore, A. M., Flynn, C. M., Froyd, K., Gesler, D. W., Hall, S. R., Hanisco, T.  
 1255 F., Hannun, R. A., Hills, A. J., Hints, E. J., Hoffman, A., Hornbrook, R. S., Huey, L. G., Hughes, S., Jimenez, J. L., Johnson, B.  
 1256 J., Katich, J. M., Keeling, R. F., Kim, M. J., Kupc, A., Lait, L. R., Lamarque, J.-F., Liu, J., McKain, K., McLaughlin, R. J.,  
 1257 Meinardi, S., Miller, D. O., Montzka, S. A., Moore, F. L., Morgan, E. J., Murphy, D. M., Murray, L. T., Nault, B. A., Neuman, J.  
 1258 A., Newman, P. A., Nicely, J. M., Pan, X., Paplawsky, W., Peischl, J., Prather, M. J., Price, D. J., Ray, E., Reeves, J. M.,  
 1259 Richardson, M., Rollins, A. W., Rosenlof, K. H., Ryerson, T. B., Scheuer, E., Schill, G. P., Schroder, J. C., Schwarz, J. P.,  
 1260 St.Clair, J. M., Steenrod, S. D., Stephens, B. B., Strode, S. A., Sweeney, C., Tanner, D., Teng, A. P., Thames, A. B., Thompson,  
 1261 C. R., Ullmann, K., Veres, P. R., Vieznor, N., Wagner, N. L., Watt, A., Weber, R., Weinzierl, B., Wennberg, P., Williamson, C.  
 1262 J., Wilson, J. C., Wolfe, G. M., Woods, C. T., and Zeng, L. H.: ATom: Merged Atmospheric Chemistry, Trace Gases, and  
 1263 Aerosols. ORNL DAAC, Oak Ridge, Tennessee, USA, <https://doi.org/10.3334/orlmdaac/1581>, 2018.
- 1264 Wolfe, G. M., Hanisco, T. F., Arkinson, H. L., Bui, T. P., Crounse, J. D., Dean-Day, J., Goldstein, A., Guenther, A., Hall, S. R.,  
 1265 Huey, G., Jacob, D. J., Karl, T., Kim, P. S., Liu, X., Marvin, M. R., Mikoviny, T., Misztal, P. K., Nguyen, T. B., Peischl, J.,  
 1266 Pollack, I., Ryerson, T., St Clair, J. M., Teng, A., Travis, K. R., Ullmann, K., Wennberg, P. O., and Wisthaler, A.: Quantifying  
 1267 sources and sinks of reactive gases in the lower atmosphere using airborne flux observations, *Geophys Res Lett*, 42, 8231-8240,  
 1268 <https://doi.org/10.1002/2015GL065839>, 2015.
- 1269 Wooldridge, P. J., Perring, A. E., Bertram, T. H., Flocke, F. M., Roberts, J. M., Singh, H. B., Huey, L. G., Thornton, J. A., Wolfe,  
 1270 G. M., Murphy, J. G., Fry, J. L., Rollins, A. W., LaFranchi, B. W., and Cohen, R. C.: Total Peroxy Nitrates ( $\Sigma$ PNs) in the  
 1271 atmosphere: the Thermal Dissociation-Laser Induced Fluorescence (TD-LIF) technique and comparisons to speciated PAN  
 1272 measurements, *Atmos. Meas. Tech.*, 3, 593-607, <https://doi.org/10.5194/amt-3-593-2010>, 2010.
- 1273 Wu, S. L., Mickley, L. J., Jacob, D. J., Logan, J. A., Yantosca, R. M., and Rind, D.: Why are there large differences between  
 1274 models in global budgets of tropospheric ozone?, *J. Geophys. Res. Atmos.*, 112, <https://doi.org/10.1029/2006jd007801>, 2007.
- 1275 Xiao, Y. P., Logan, J. A., Jacob, D. J., Hudman, R. C., Yantosca, R., and Blake, D. R.: Global budget of ethane and regional  
 1276 constraints on US sources, *J. Geophys. Res. Atmos.*, 113, <https://doi.org/10.1029/2007jd009415>, 2008.
- 1277 Yacovitch, T. I., Herndon, S. C., Roscioli, J. R., Floerchinger, C., McGovern, R. M., Agnese, M., Petron, G., Kofler, J., Sweeney,  
 1278 C., Karion, A., Conley, S. A., Kort, E. A., Nahle, L., Fischer, M., Hildebrandt, L., Koeth, J., McManus, J. B., Nelson, D. D.,  
 1279 Zahniser, M. S., and Kolb, C. E.: Demonstration of an ethane spectrometer for methane source identification, *Environ. Sci.*  
 1280 *Technol.*, 48, 8028-8034, <http://doi.org/10.1021/es501475q>, 2014.
- 1281 Yang, M., Nightingale, P. D., Beale, R., Liss, P. S., Blomquist, B., and Fairall, C.: Atmospheric deposition of methanol over the  
 1282 Atlantic Ocean, *Proc. Natl. Acad. Sci. U.S.A.*, 110, 20034-20039, <https://doi.org/10.1073/pnas.1317840110>, 2013.

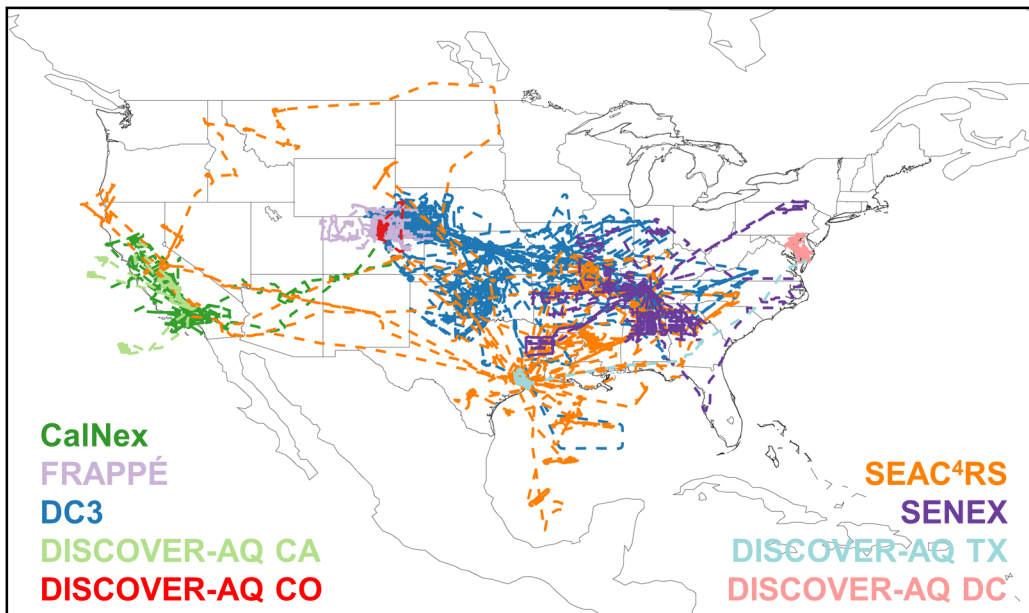
- 1283 Yang, M., Beale, R., Liss, P., Johnson, M., Blomquist, B., and Nightingale, P.: Air-sea fluxes of oxygenated volatile organic  
1284 compounds across the Atlantic Ocean, *Atmos. Chem. Phys.*, 14, 7499-7517, <https://doi.org/10.5194/acp-14-7499-2014>, 2014a.
- 1285 Yang, M. X., Blomquist, B. W., and Nightingale, P. D.: Air-sea exchange of methanol and acetone during HiWinGS: Estimation  
1286 of air phase, water phase gas transfer velocities, *J. Geophys. Res. Oceans*, 119, 7308-7323,  
1287 <https://doi.org/10.1002/2014JC010227>, 2014b.
- 1288 Yevich, R., and Logan, J. A.: An assessment of biofuel use and burning of agricultural waste in the developing world, *Global*  
1289 *Biogeochem Cy*, 17, <https://doi.org/10.1029/2002gb001952>, 2003.
- 1290 Yu, K., Keller, C. A., Jacob, D. J., Molod, A. M., Eastham, S. D., and Long, M. S.: Errors and improvements in the use of  
1291 archived meteorological data for chemical transport modeling: an analysis using GEOS-Chem v11-01 driven by GEOS-5  
1292 meteorology, *Geosci Model Dev*, 11, 305-319, <https://doi.org/10.5194/gmd-11-305-2018>, 2018.
- 1293 Yu, K. R., Jacob, D. J., Fisher, J. A., Kim, P. S., Marais, E. A., Miller, C. C., Travis, K. R., Zhu, L., Yantosca, R. M., Sulprizio,  
1294 M. P., Cohen, R. C., Dibb, J. E., Fried, A., Mikoviny, T., Ryerson, T. B., Wennberg, P. O., and Wisthaler, A.: Sensitivity to grid  
1295 resolution in the ability of a chemical transport model to simulate observed oxidant chemistry under high-isoprene conditions,  
1296 *Atmos. Chem. Phys.*, 16, 4369-4378, <https://doi.org/10.5194/acp-16-4369-2016>, 2016.
- 1297 Zheng, W., Flocke, F. M., Tyndall, G. S., Swanson, A., Orlando, J. J., Roberts, J. M., Huey, L. G., and Tanner, D. J.:  
1298 Characterization of a thermal decomposition chemical ionization mass spectrometer for the measurement of peroxy acyl nitrates  
1299 (PANs) in the atmosphere, *Atmos. Chem. Phys.*, 11, 6529-6547, <https://doi.org/10.5194/acp-11-6529-2011>, 2011.
- 1300 Zhou, X. L., and Mopper, K.: Photochemical production of low-molecular-weight carbonyl compounds in seawater and surface  
1301 microlayer and their air-sea exchange, *Mar. Chem.*, 56, 201-213, [https://doi.org/10.1016/S0304-4203\(96\)00076-X](https://doi.org/10.1016/S0304-4203(96)00076-X), 1997.
- 1302 Zhu, L., Jacob, D. J., Kim, P. S., Fisher, J. A., Yu, K., Travis, K. R., Mickley, L. J., Yantosca, R. M., Sulprizio, M. P., De Smedt,  
1303 I., Abad, G. G., Chance, K., Li, C., Ferrare, R., Fried, A., Hair, J. W., Hanisco, T. F., Richter, D., Scarino, A. J., Walega, J.,  
1304 Weibring, P., and Wolfe, G. M.: Observing atmospheric formaldehyde (HCHO) from space: validation and intercomparison of  
1305 six retrievals from four satellites (OMI, GOME2A, GOME2B, OMPS) with SEAC(4)RS aircraft observations over the Southeast  
1306 US, *Atmos. Chem. Phys.*, 16, 13477-13490, <https://doi.org/10.5194/acp-16-13477-2016>, 2016.
- 1307 Zhuang, J. W., Jacob, D. J., and Eastham, S. D.: The importance of vertical resolution in the free troposphere for modeling  
1308 intercontinental plumes, *Atmos. Chem. Phys.*, 18, 6039-6055, <https://doi.org/10.5194/acp-18-6039-2018>, 2018.
- 1309

1310 **Table 1. Overview of aircraft campaigns used here<sup>a</sup>.**

	Aircraft platform	Aircraft ceiling	Timeframe	Sampling region	Campaign overview and data DOI if applicable
CalNex	NOAA WP-3D	7600m	May – Jul 2010	California and offshore	Ryerson et al. (2013)
DC3	NASA DC-8	12500m	May – Jun 2012	Northeastern Colorado, west Texas to central Oklahoma, and northern Alabama	Barth et al. (2015) DC3 Science Team (2013)
	NSF/NCAR GV	15500m			
SEAC <sup>4</sup> RS	NOAA WP-3D	7600m	Jun – Jul 2013	Southeastern US	Warneke et al. (2016)
SEAC <sup>4</sup> RS	NASA DC-8	12500m	Aug – Sep 2013	Southeastern US and Gulf of Mexico	Toon et al. (2016) SEAC <sup>4</sup> RS Science Team (2013)
DISCOVER-AQ	NASA P-3B	8500m	Jun – Jul 2011	Baltimore-Washington, D.C.	Crawford and Pickering (2014) DISCOVER-AQ Science Team (2014)
			Jan – Feb 2013	San Joaquin Valley, California	
			Sep 2013	Houston, Texas	
			Jul – Aug 2014	Denver, Colorado	
FRAPPÉ	NCAR C-130	7900m	Jul – Aug 2014	Northern Colorado	Pfister et al. (2017)

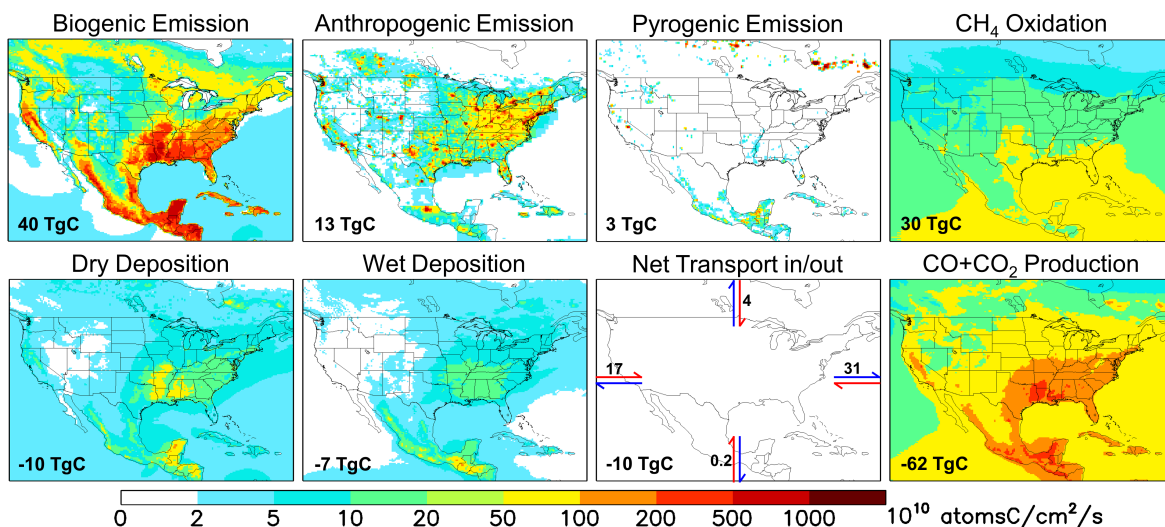
<sup>a</sup>See measurement details in Table S1 (O’Sullivan et al., 2018; Treadaway et al., 2018; Lerner et al., 2017; Min et al., 2016; Müller et al., 2016b; Cazorla et al., 2015; Richter et al., 2015; Lee et al., 2014; Müller et al., 2014; Yacovitch et al., 2014; Kaser et al., 2013; DiGangi et al., 2011; Fried et al., 2011; Zheng et al., 2011; Apel et al., 2010; Pollack et al., 2010; St Clair et al., 2010; Weibring et al., 2010; Wooldridge et al., 2010; Gilman et al., 2009; Hottle et al., 2009; Osthoff et al., 2008; de Gouw and Warneke, 2007; Huey, 2007; Kim et al., 2007; Crouse et al., 2006; Slusher et al., 2004; Blake et al., 2003; Schauffler et al., 2003; Wisthaler et al., 2002; Colman et al., 2001; Ryerson et al., 1999; Ryerson et al., 1998; Weinheimer et al., 1994).

1311  
1312  
1313  
1314

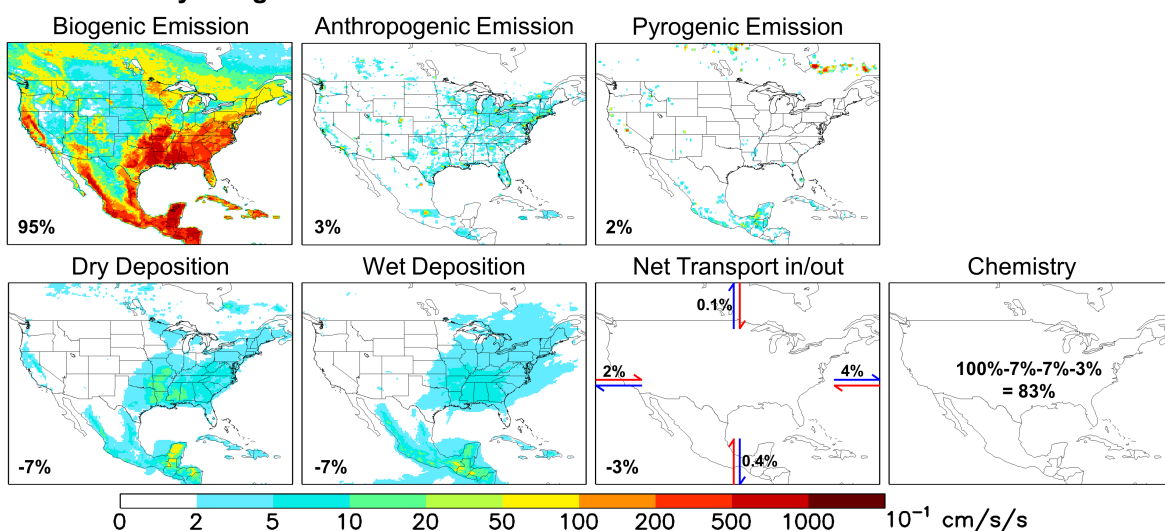


1315  
1316 **Figure 1. Flight tracks for the aircraft campaigns used in this study: CalNex (May-Jun 2010), FRAPPÉ (Jul-**  
1317 **Aug 2014), DC3 (May-Jun 2012), DISCOVER-AQ CA (Jan-Feb 2013), DISCOVER-AQ CO (Jul-Aug 2014),**  
1318 **SEAC<sup>4</sup>RS (Aug-Sep 2013), SENEX (Jun 2013), DISCOVER-AQ TX (Sep 2013), and DISCOVER-AQ DC**  
1319 **(Jun-Jul 2011).**

**(a) VOC Carbon Budget**



**(b) VOC Reactivity Budget**

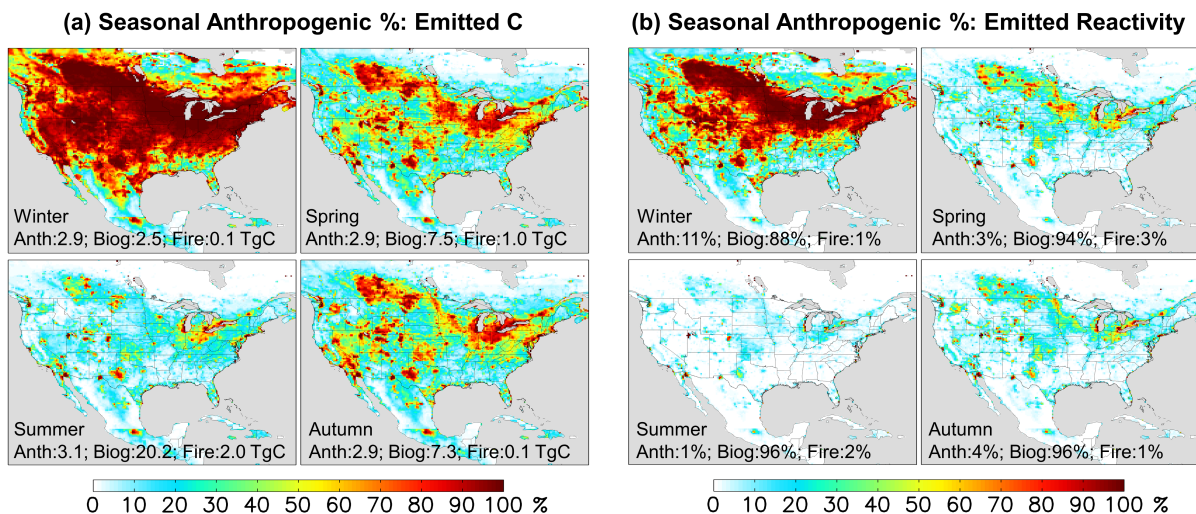


1320

1321 **Figure 2. Annual VOC-carbon (a) and reactivity (b) budgets over North America as simulated by GEOS-**  
 1322 **Chem for 2013. For panel (a) the annually integrated flux for each source/sink is given inset. For panel (b) all**  
 1323 **VOC fluxes are weighted by the corresponding OH reaction rate coefficient at 298 K to derive a VOC**  
 1324 **reactivity budget. Values inset indicate the fraction of total emitted reactivity produced or removed by that**  
 1325 **source/sink/transport process. Positive fluxes denote sources and negative fluxes denote sinks.**

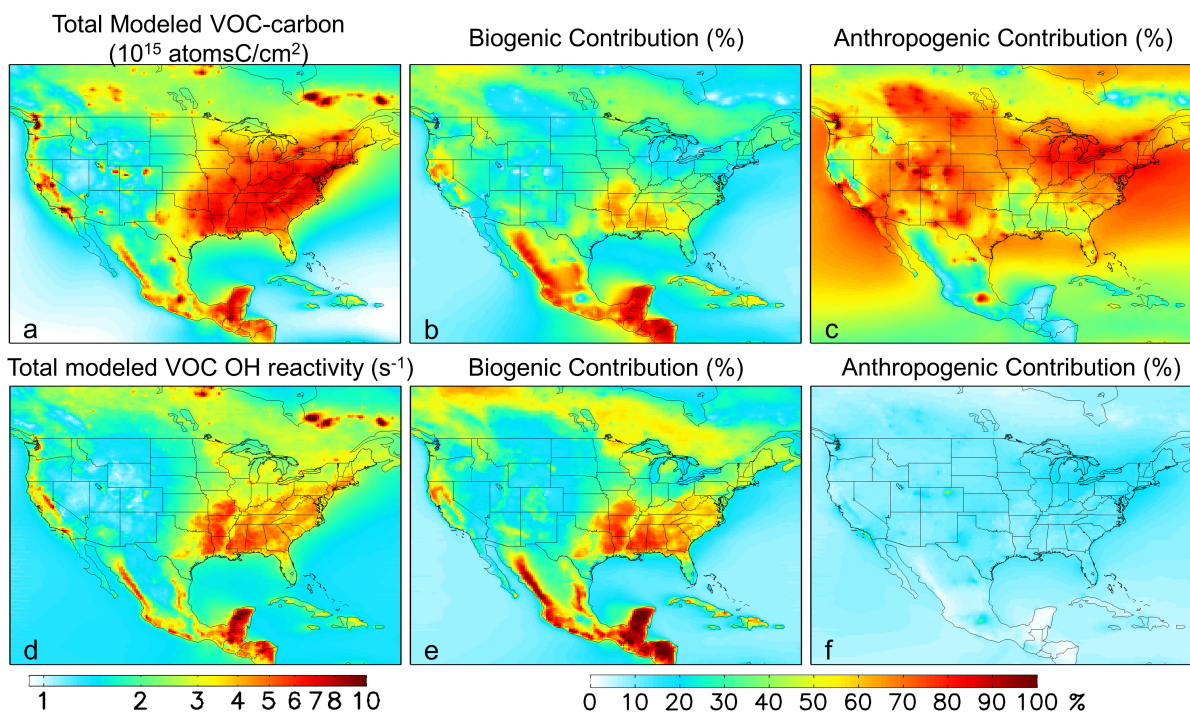
1326



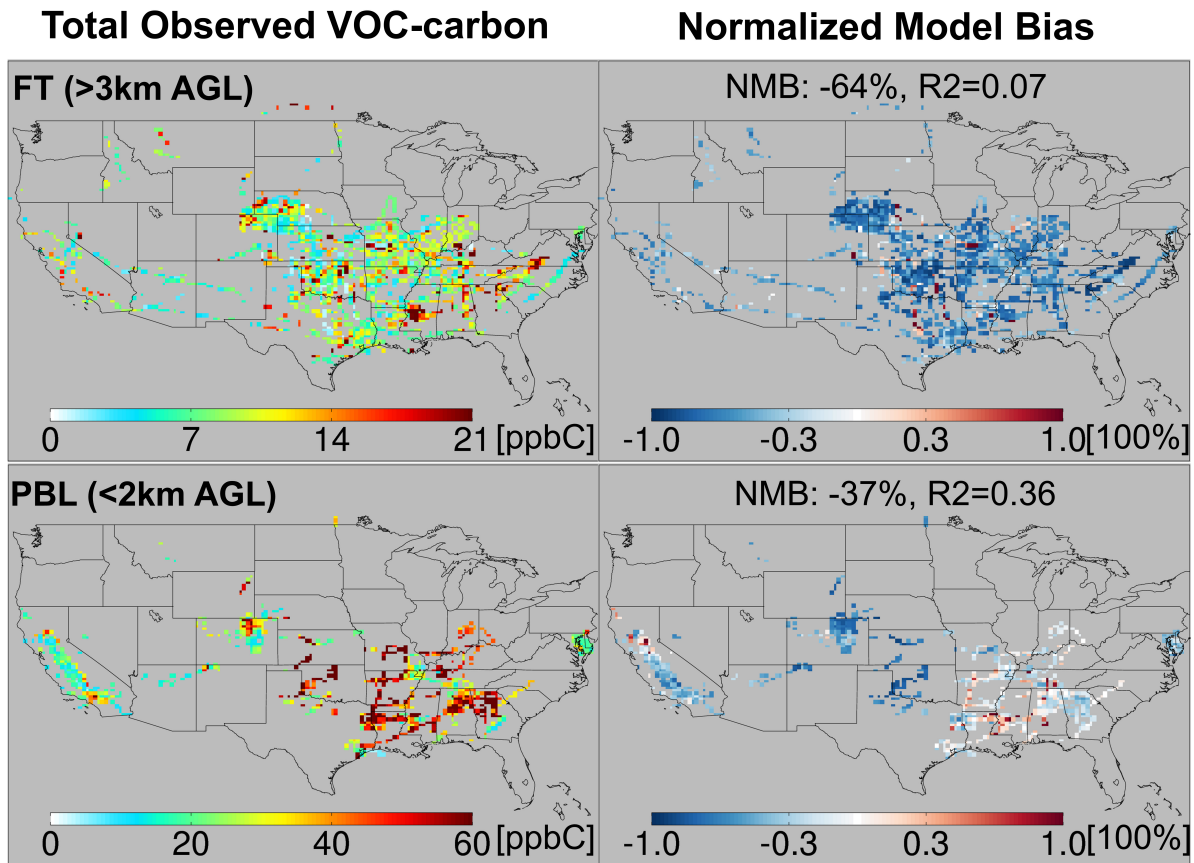


1327  
 1328 **Figure 3. Seasonal anthropogenic contribution to total VOC-carbon emissions (panel a) and to total**  
 1329 **reactivity-weighted VOC emissions (panel b). Numbers inset indicate the domain-aggregated emissions (panel**  
 1330 **a) or domain-wide contribution to reactivity-weighted emissions (panel b) from anthropogenic, biogenic, and**  
 1331 **biomass burning sources.**

1332

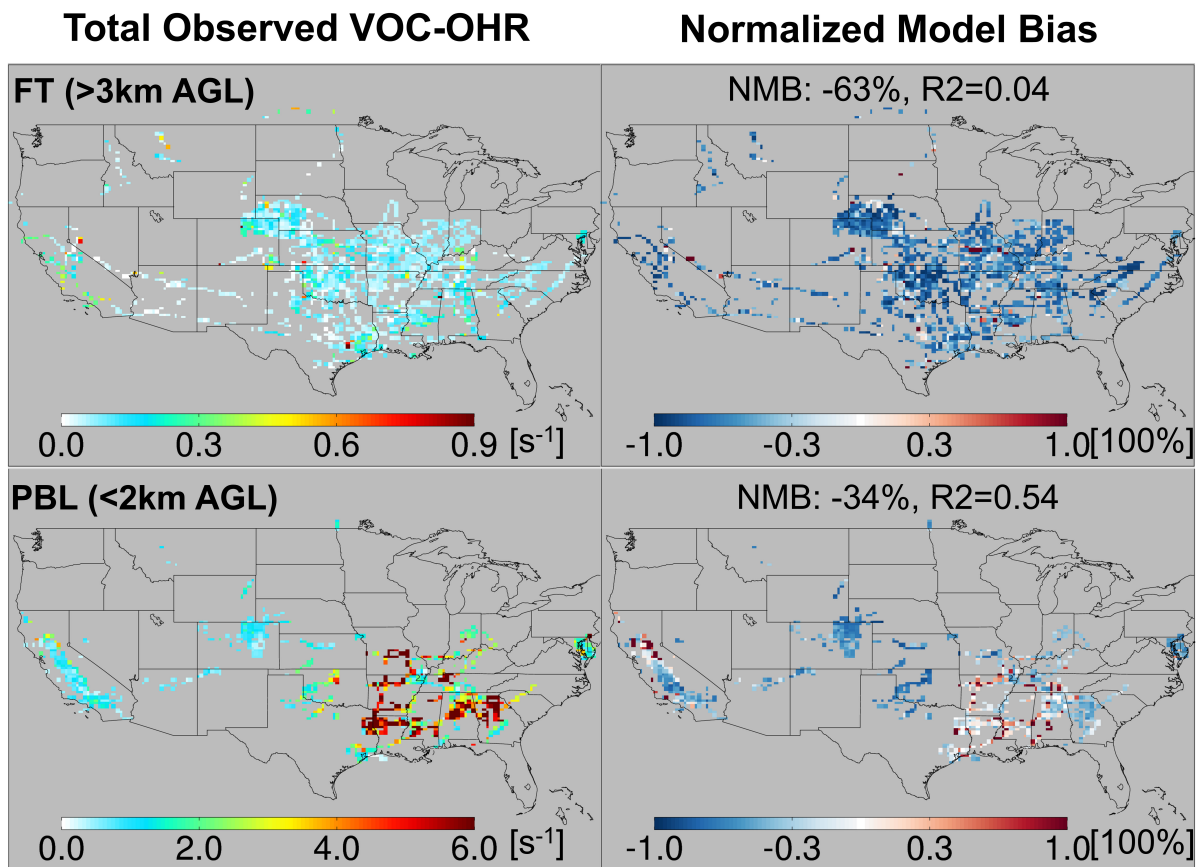


1333  
 1334 **Figure 4. Distribution and source attribution of ambient VOC-carbon and associated OH reactivity over**  
 1335 **North America. Panels (a) and (d): total VOC-carbon and VOC-driven OH reactivity as simulated in the**  
 1336 **lowest model layer (below ~130m). Panel (b) and (e): ambient VOC-carbon and reactivity attributed to**  
 1337 **biogenic VOC emissions. Panel (c) and (f): ambient VOC-carbon and reactivity attributed to anthropogenic**  
 1338 **VOC emissions. Source attributions are derived based on model sensitivity tests with 10% modified**  
 1339 **anthropogenic or biogenic emissions, as described in-text.**



1340

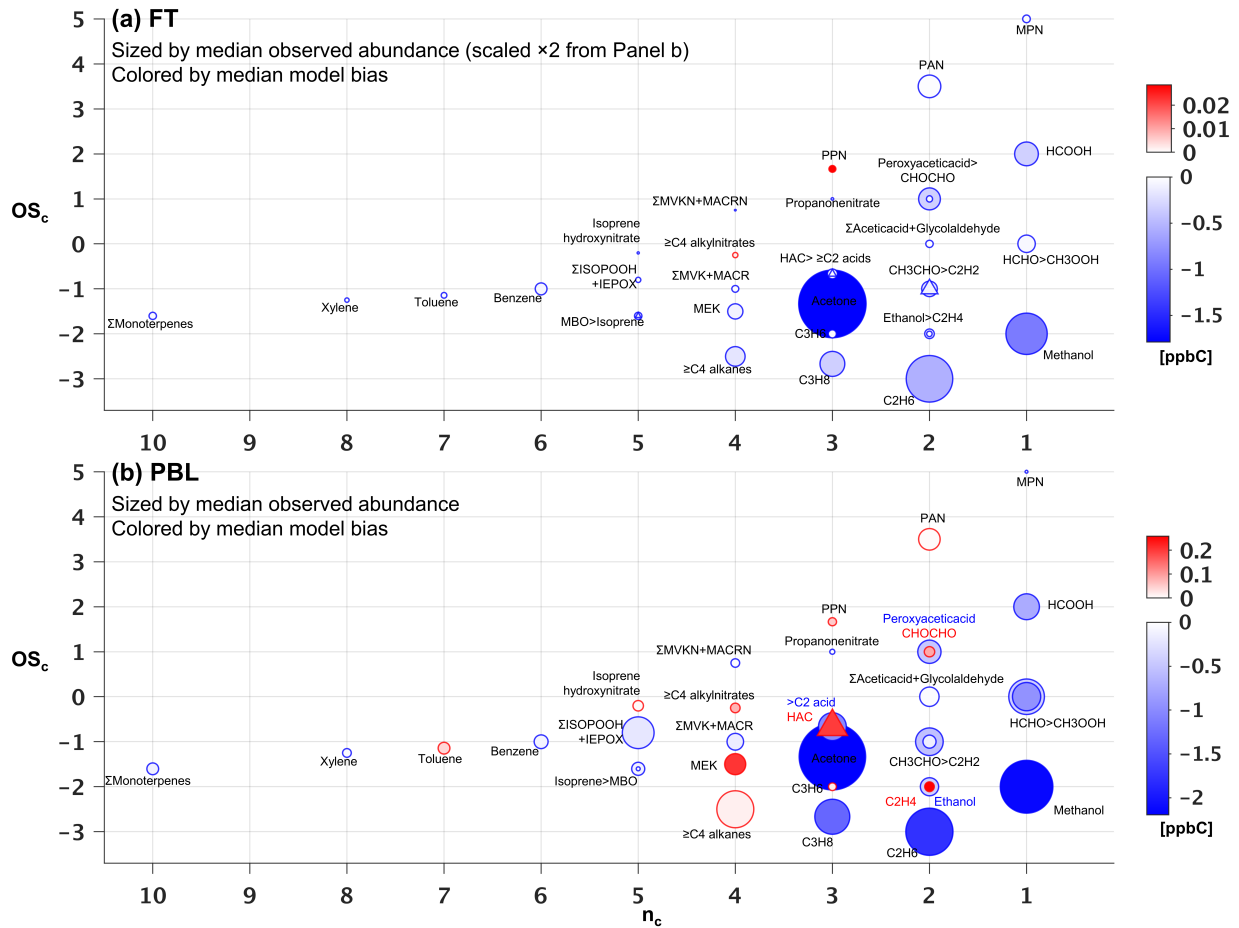
1341 **Figure 5. Total observed VOC-carbon loading (left) over North America in the planetary boundary layer (<2**  
 1342 **km AGL) and free troposphere (>3 km AGL). In the right-hand panels the GEOS-Chem model simulation is**  
 1343 **compared to co-located aircraft observation with the normalized mean bias given inset. Note that the**  
 1344 **sampling season and instrument payload vary among campaigns.**



1345

1346 **Figure 6. Total observed VOC reactivity (left) over North America in the planetary boundary layer (<2 km**  
 1347 **AGL) and free troposphere (>3 km AGL). In the right-hand panels, the GEOS-Chem model simulation is**  
 1348 **compared to co-located aircraft observation with the normalized mean bias given inset. Note that the**  
 1349 **sampling season and instrument payload vary among campaigns.**

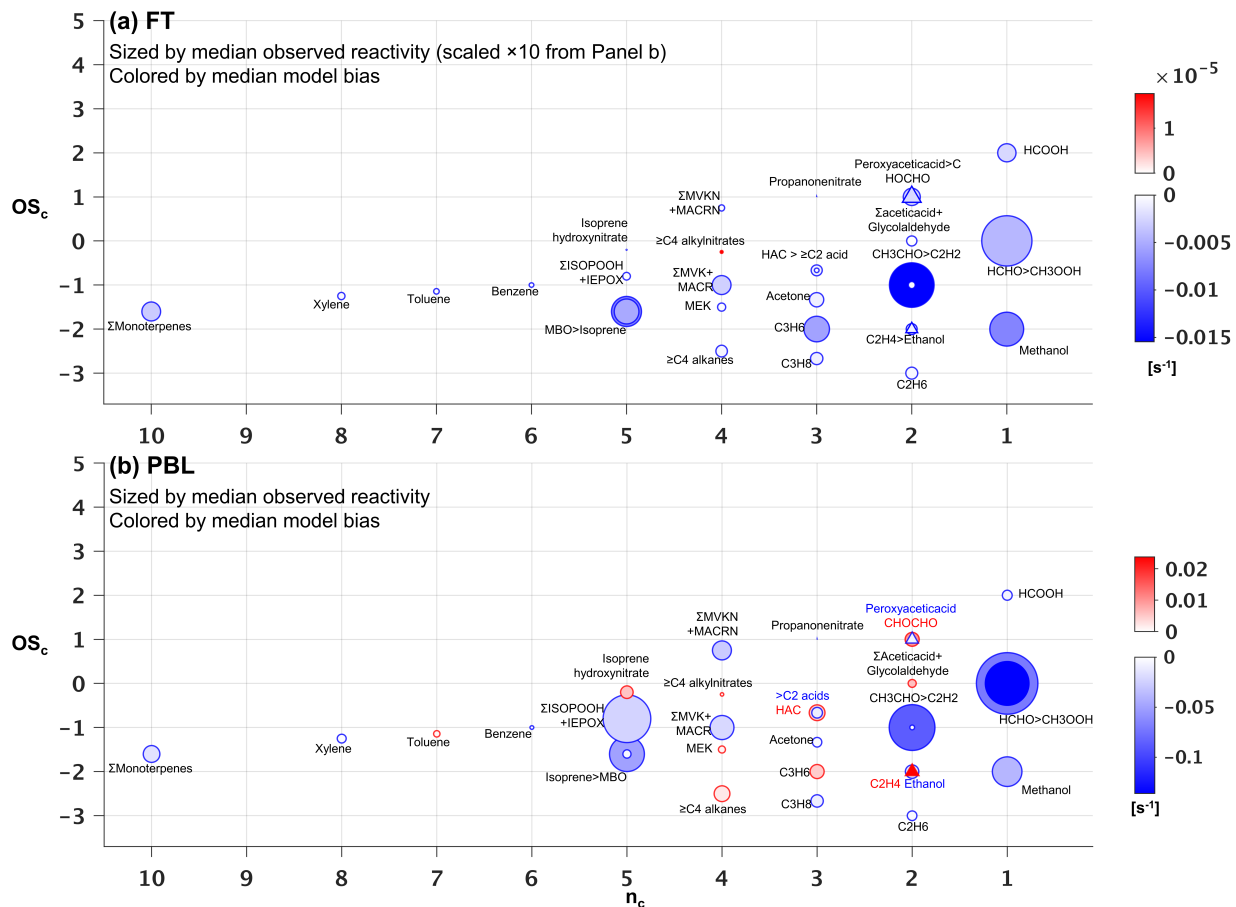
1350



1351

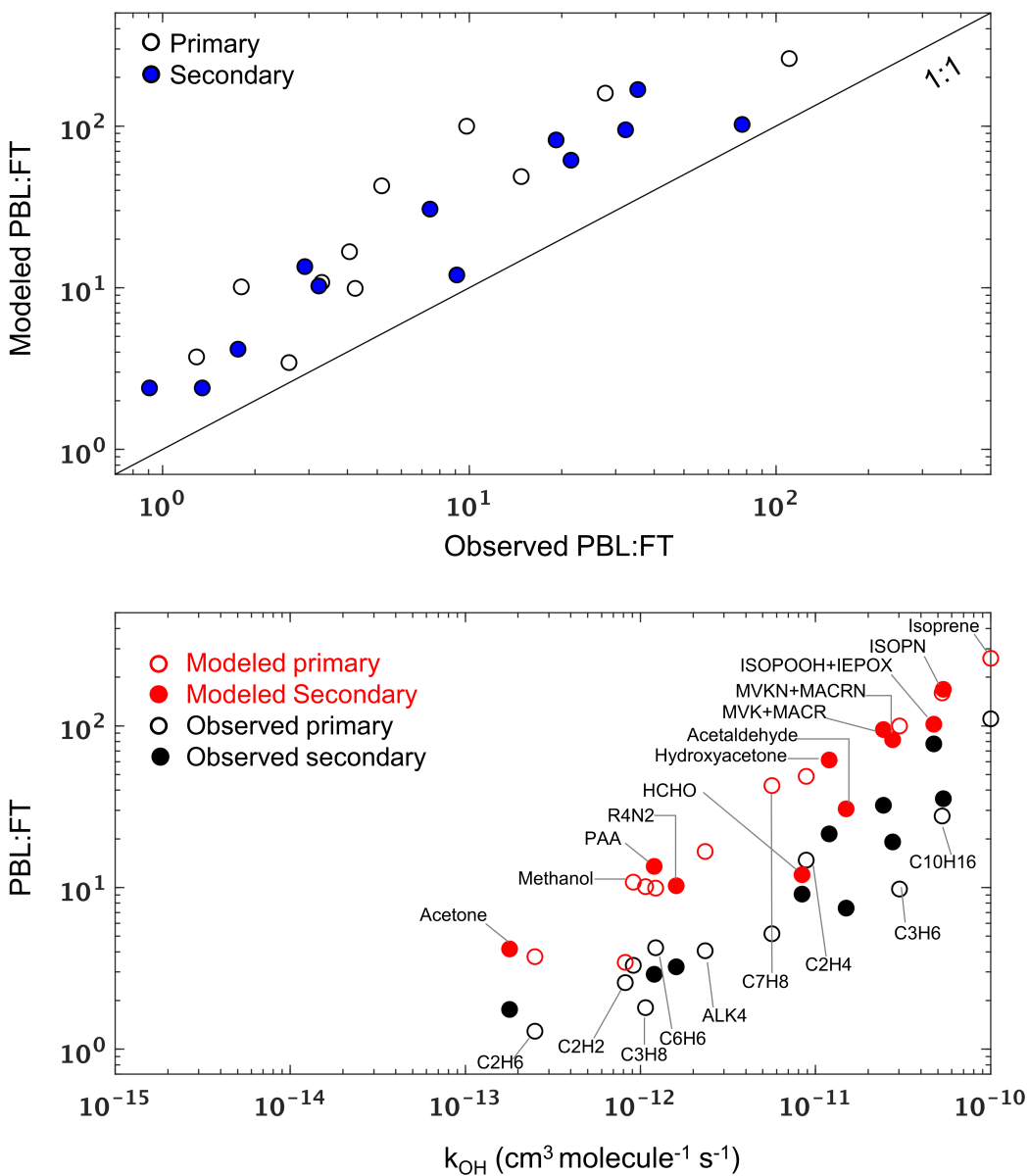
1352 **Figure 7. Observed versus predicted VOC-carbon as a function of carbon oxidation state ( $OS_c$ ) and number**  
 1353 **of carbon atoms ( $n_c$ ). Each circle indicates a single VOC (or lumped category for those that are measured or**  
 1354 **modeled collectively). Symbols are sized according to the observed median abundance (ppbC) of each species**  
 1355 **in the FT (panel a) and in the PBL (panel b, note altered size scaling from Panel a). Triangles are used when**  
 1356 **co-located circles are too close in size to distinguish, and symbols are colored according to the median**  
 1357 **absolute model bias in each case. For overlapping species, the more abundant of the two is indicated with “>”.**





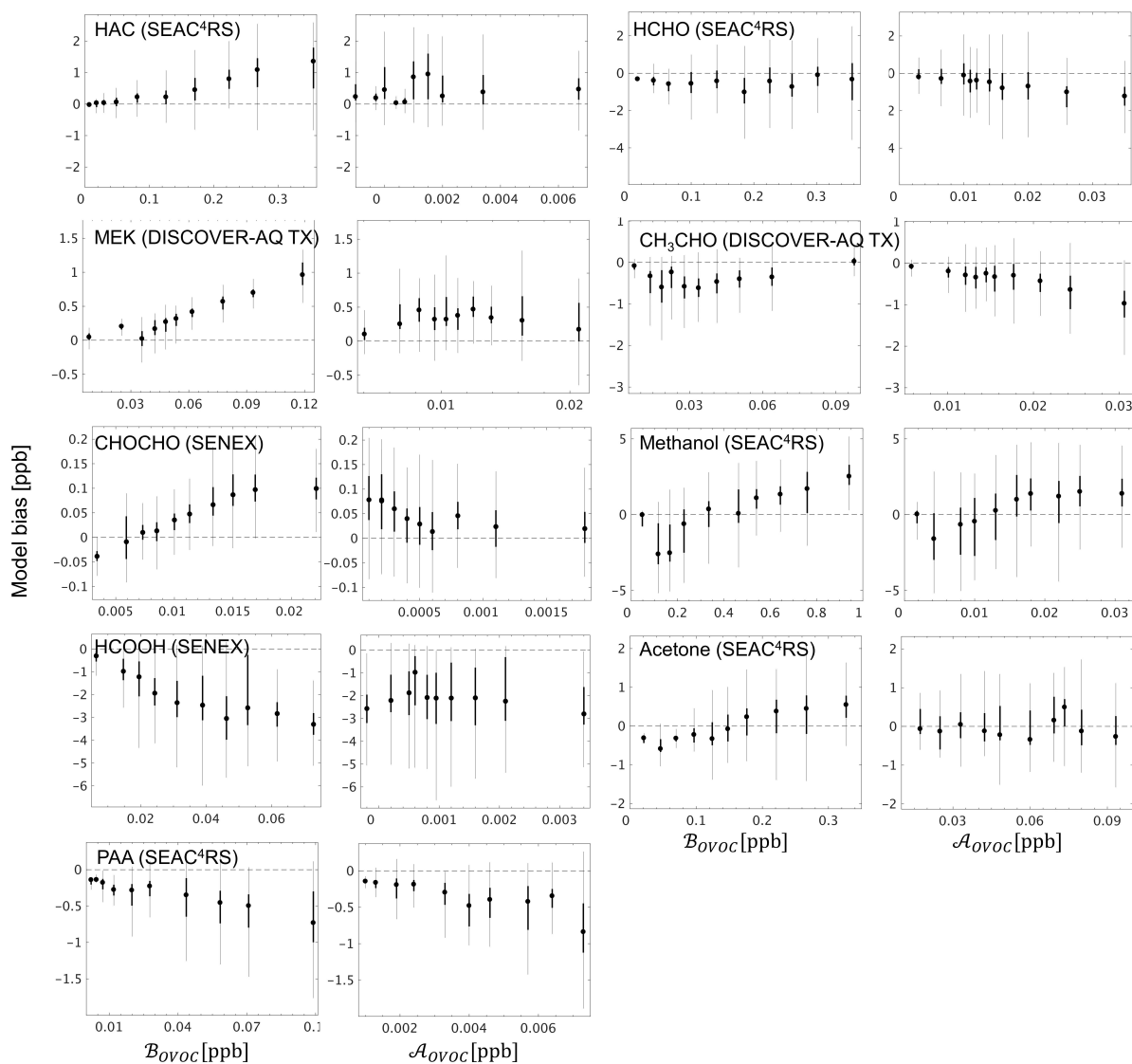
1358

1359 **Figure 8. Observed versus predicted VOC reactivity as a function of carbon oxidation state ( $OS_c$ ) and**  
 1360 **number of carbon atoms ( $n_c$ ). Each circle indicates a single VOC (or lumped category for those that are**  
 1361 **measured or modeled collectively). Symbols are sized according to the observed median reactivity ( $s^{-1}$ ) of each**  
 1362 **species in the FT (Panel a) and in the PBL (Panel b, note altered size scaling from Panel a). Triangles are used**  
 1363 **when co-located circles are too close in size to distinguish, and symbols are colored according to the median**  
 1364 **absolute model bias in each case. For overlapping species, the more abundant of the two is indicated with “>”.**



1365

1366 **Figure 9. Top panel: Modeled versus observed mean PBL:FT ratio (mixing ratio units) for each VOC during**  
 1367 **the SEAC<sup>4</sup>RS campaign. Each datapoint represents a single VOC, and the 1:1 line is also shown. Bottom**  
 1368 **panel: Modeled and observed mean PBL:FT ratio for VOCs during SEAC<sup>4</sup>RS as a function of their OH**  
 1369 **reaction rate coefficient at 298K. In both panels, unfilled and filled symbols indicate species with**  
 1370 **predominantly primary and secondary sources, respectively.**



1371

1372 **Figure 10. GEOS-Chem model bias for select OVOCs in the boundary layer (<1 km here), binned according**  
 1373 **to the contribution from biogenic ( $B_{OVOC}$ ) and anthropogenic ( $A_{OVOC}$ ) sources to the overall abundance.**  
 1374  **$B_{OVOC}$  and  $A_{OVOC}$  represent the integrated influence of primary + secondary biogenic and anthropogenic**  
 1375 **sources (respectively) for a given OVOC along the aircraft flight track based on the model simulation, as**  
 1376 **described in-text. The 10 plotted bins each represent an equal number of datapoints for a given OVOC, with**  
 1377 **the box plots indicating the corresponding median (filled circle), interquartile range (thick line), and 99%**  
 1378 **confidence interval (thin line).**